

Synthesis, silver-etching, and light scattering study of gold-silver alloy nanoparticles

Xingming Situ

Department of Chemistry
McGill University, Montreal

April 2022

A thesis submitted to McGill University in partial fulfillment of the
requirements for the degree of

Master of Science

© 2022 Xingming Situ

ABSTRACT

This thesis concerns the synthesis, etching, and Rayleigh scattering of gold-silver alloy nanoparticles. We report a novel two-step method for the synthesis of uniform quasi-spherical and monodisperse gold-silver alloy nanoparticles with diameters around 80 nm. Our method makes use of gold acetate (rather than chloroauric acid) as a gold precursor to avoid the formation of silver chloride precipitates during synthesis. Gold and silver are distributed uniformly within the cores of all Au-Ag alloy nanoparticles, while the surface is enriched in silver. This silver enriched surface layer is thicker and more prominent for 25% Au alloy nanoparticles than for 50% and 75% Au alloy nanoparticles.

Inspired by previous work studying the mechanism of photo-mediated triangular silver nanoprism growth, where the oxidative dissolution of small silver particles was facilitated by Bis(*p*-sulfonatophenyl)phenylphosphine dihydrate dipotassium (BSPP), we investigate silver etching of our alloy nanoparticles. Our measurements show that a novel nanostructure is formed after etching where smaller nanoparticles are deposited on the surface of gold-silver alloy nanoparticles.

Finally, we present some preliminary results of Rayleigh scattering measurements on our synthesized gold-silver alloy nanoparticles with dark-field hyperspectral microscope at the individual nanoparticle level. This study is at a very early stage and aims at investigating how uniform our alloy nanoparticles are with respect to element distributions in order to understand their plasmonic properties.

RÉSUMÉ

Cette thèse concerne la synthèse, la gravure et la diffusion Rayleigh de nanoparticules d'alliage Au-Ag. Nous rapportons une nouvelle méthode en deux étapes pour la synthèse de uniformes nanoparticules d'alliage Au-Ag quasi-sphériques et monodisperses avec des diamètres d'environ 80 nm. Notre méthode utilise l'acétate d'or (plutôt que l'acide chloraurique) comme précurseur d'or pour éviter la formation de précipités de chlorure d'argent lors de la synthèse. L'or et l'argent sont répartis uniformément dans les noyaux de toutes les nanoparticules d'alliage Au-Ag, tandis que la surface est enrichie en argent. Cette couche de surface enrichie en argent est plus épaisse et plus proéminente pour les nanoparticules d'alliage à 25 % Au que pour les nanoparticules d'alliage à 50 % et 75 % Au.

Inspirés par des travaux antérieurs étudiant le mécanisme de la croissance de nanoprismes d'argent triangulaires photomédiés, où la dissolution oxydative de petites particules d'argent était facilitée par le Bis(p-sulfonatophenyl)phenylphosphine dihydrate dipotassium (BSPP), nous étudions la gravure de l'argent de nos nanoparticules d'alliage Au-Ag. Nos mesures montrent qu'une nouvelle nanostructure se forme après la gravure où des nanoparticules plus petites sont déposées à la surface des nanoparticules d'alliage Au-Ag.

Enfin, nous présentons quelques résultats préliminaires de mesures de diffusion de Rayleigh sur nos nanoparticules d'alliage Au-Ag synthétisées avec un microscope hyperspectral à fond noir au niveau des nanoparticules individuelles. Cette étude est à un stade très précoce et vise à étudier l'uniformité de nos nanoparticules d'alliage en ce

qui concerne les distributions d'éléments afin de comprendre leurs propriétés plasmoniques.

ACKNOWLEDGEMENTS

First and foremost, I would like to express my sincere gratitude to my supervisor, Dr. Amy Szuchmacher Blum, for her continuous support, guidance, suggestions, and optimism over the past four years. Dr. Blum's enthusiasm and dedication to teaching and research are admirable and inspiring. A lot of active, timely and insightful feedback she provides with me has promoted my research progress while still offering me plenty of room for my own ideas. It is my great honour and pleasure to conduct research work over the past years in Blum Lab, which is a fruitful journey. And I am also grateful to my committee members, Dr. Audrey Moores and Dr. Linda Reven, who provide a great deal of helpful and friendly advice on my research.

Secondly, I would like to thank my colleagues in Blum Lab, Shoronia Cross, Dan Petrescu, Ish Abu-Baker, Alex Al-Feghali and Guido Merino. I really appreciate the help and happiness from my colleagues, especially attending MRS 2019 Fall meeting in Boston with Dan. Thanks to Dr. Jun Zhu, who I learn many research skills from. Thank you, Dr. David Liu, who is very resourceful and helps me with TEM and STEM imaging. Thank you, Chantal Marotte, who continuously sends useful information and friendly reminders to every graduate student in Department of Chemistry, keeping me on track in fulfilling the course and research requirements.

Finally, deep thanks go to my families both in Canada and China. Thanks for your unconditional love and support. Without you, I would never have had the opportunity to be part of McGill community. Hopefully, we could reunite in the near future of 2022.

TABLE OF CONTENTS

ABSTRACT	ii
RÉSUMÉ	iii
ACKNOWLEDGEMENTS	v
TABLE OF CONTENTS	vii
CONTRIBUTION OF AUTHORS	ix
1. GENERAL INTRODUCTION	1
1.1 Plasmons of nanoparticles	1
1.2 Synthesis of gold-silver alloy nanoparticles	3
1.3 Applications of gold-silver alloy nanoparticles	8
1.4 Conclusion	12
1.5 Reference	13
2. TWO-STEP SYNTHESIS OF GOLD-SILVER ALLOY NANOPARTICLES VIA THE COMBINATION OF SEEDED GROWTH AND CITRATE CO-REDUCTION	17
2.1 Introduction	17
2.2 Experimental	20
2.3 Results and Discussion	23
2.4 Conclusion	30
2.5 Reference	32

3. THE DEALLOYING OF GOLD-SILVER ALLOY NANOPARTICLES BY BSPP TOWARDS POROUS NANOSTRUCTURES	37
3.1 Introduction	37
3.2 Experimental	39
3.3 Results and Discussion	41
3.4 Preliminary Conclusion and Future Work	47
3.5 Reference	49
4. INVESTIGATION OF THE OPTICAL PROPERTIES OF GOLD-SILVER ALLOY NANOPARTICLES WITH DARK-FIELD HYPERSPECTRAL MICROSCOPY	51
4.1 Introduction	51
4.2 Experimental	54
4.3 Results and Discussion	57
4.4 Preliminary Conclusion and Future Work	62
4.5 Reference	64
5. CONCLUDING REMARKS AND FUTURE DIRECTIONS	66

CONTRIBUTION OF AUTHORS

Chapter Two: Xingming Situ, Serene Bayram and Amy Szuchmacher Blum.

Xingming Situ developed the methodology for the preparation of gold-silver alloy nanoparticles by seeded growth and citrate co-reduction. Xingming Situ measured the UV-Vis extinction spectra of gold-silver alloy nanoparticles and conducted TEM and EDX measurements. Serene Bayram and Amy Szuchmacher Blum provided the idea of using gold acetate rather than chloroauric acid as gold precursors.

Amy Szuchmacher Blum offered intellectual guidance, experiment results interpretation and support on experimental design and implementation. Xingming Situ wrote the manuscript and all authors reviewed and revised the manuscript.

Chapter Three: Xingming Situ, Serene Bayram and Amy Szuchmacher Blum.

Serene Bayram and Amy Szuchmacher Blum designed the dealloying reaction.

Xingming Situ optimized the experiment design and continued this research project by measuring UV-Vis extinction spectra of BSPP-treated gold-silver alloy nanoparticles over time and analyzing the BSPP-treated alloy nanoparticles based on TEM images and EDX-mapping results. Xingming Situ proposed a dealloying reaction mechanism.

Amy Szuchmacher Blum provided guidance on experiment set-up, experiment data analysis and interpretation. Xingming Situ wrote this chapter and Amy Szuchmacher Blum reviewed and revised this chapter.

Chapter Four: Xingming Situ, Alexander Al-Feghali and Amy Szuchmacher Blum.

Xingming Situ conducted the dark-field hyperspectral microscopy measurement of gold-silver alloy nanoparticles and analyzed the experimental data. Alexander Al-Feghali developed the procedures for glass slide pre-treatment and sample preparation. Amy Szuchmacher Blum offered feedback and support regarding the use of dark-field microscopy and measurement data analysis.

Xingming Situ wrote this chapter and Amy Szuchmacher Blum reviewed and revised this chapter.

Chapter 1. General introduction

1.1 Plasmons of nanoparticles

Plasmons are collective oscillations of free electrons in metals¹. According to the Fermi liquid model, plasmons can be described as a negatively charged electron cloud coherently displaced from its equilibrium position around a lattice made of positively charged ions, in analogy to a real plasma². The plasmons in metals can be classified as bulk plasmon (from bulk metal), propagating surface plasmon polaritons (from metal surfaces) and localized surface plasmons³ (from metallic nanoparticles). Nanoparticles are defined as particles composed of a certain number of atoms ranging from 3 to 10^7 and they feature properties that are neither those of molecules nor those of the bulk material⁴. Plasmons in nanoparticles with sizes much smaller than the photon wavelength are non-propagating excitations, called localized surface plasmons, because the resulting plasmon oscillation is distributed over the whole particle volume³ (Figure 1). Only light with frequency in resonance with the collective oscillations of free electrons is able to excite the localized surface plasmon¹. The plasmon resonance of nanoparticles has generated enormous scientific interest, including in biological microscopy⁵, medicine⁶, and sensors⁷.

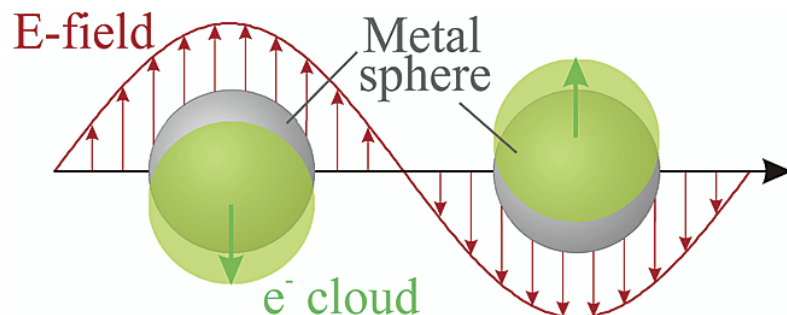


Figure 1. Schematic of plasmon oscillation for a spherical nanoparticle, showing the displacement of the conduction electron charge cloud relative to the nuclei⁸. Reprinted with permission from⁸. Copyright (2003) American Chemical Society.

As the coherent displacements of electrons from the positively charged lattice generates a restoring force that pulls the polarized electrons back to the lattice, the plasmons in nanoparticles can be considered as a mass-spring harmonic oscillator driven by the energy of resonant light wave³. Measuring the extinction spectra of plasmonic nanoparticles is commonly used to study their properties and the extinction intensity is composed of scattering intensity and absorption intensity. Based on Mie theory for a plasmonic nanosphere, the extinction cross section could be expressed as⁴:

$$C_{ext} = \frac{24\pi^2 R^3 \varepsilon_m^{2/3}}{\lambda} \frac{\varepsilon_2}{(\varepsilon_1 + 2\varepsilon_m)^2 + \varepsilon_2^2}$$

where R is the radius of particles, λ is the light wavelength, ε_m is the dielectric constant of the non-absorbing surrounding medium, and ε is the nanoparticle's complex dielectric function: $\varepsilon = \varepsilon_1 + i\varepsilon_2$. From the equation above, it is apparent that the dielectric constant (ε_m) of the surrounding medium plays a predominant role in determining both the plasmon peak position and intensity⁴ because the extinction cross section's quantity reaches a maximum for $\varepsilon_1 = -2\varepsilon_m$ ⁹ and ε is dependent on the frequency of incident light. Secondly, the increase in nanoparticle diameter not only leads to an increase in plasmon resonance intensity, but also to a red-shift of the plasmonic band position in noble metals¹⁰ since R modifies the expression of the dielectric constant of the metal⁴. Lastly,

core-shell nanoparticles' spectral characteristics can be efficiently treated with the Mie model¹¹ while alloy nanoparticles' can not be predicted by this model¹². For non-spherical plasmonic nanostructures including nanorods, nanoprisms and polyhedral nanoparticles, numerical methods such as discrete dipole approximation (DDA), the T-matrix method, finite-difference time-domain (FDTD) simulations, finite element calculations, and finite element calculations are used for the calculations of spectral characteristics of these nanostructures¹³.

1.2 Synthesis of gold-silver alloy nanoparticles

Bimetallic nanoparticles, with different compositions and structures compared to their pure elemental nanoparticle counterparts, demonstrate different optical and catalytic properties and become a popular domain for research¹⁴⁻¹⁶. Among various bimetallic nanoparticles, gold-silver alloy nanoparticles attract great attention by virtue of their remarkable optical properties¹⁷. For instance, the Lycurgus Cup (Figure 2), a 4th century Roman glass cage cup with dichroic effect, is colored by cuboidal gold-silver alloy nanoparticles of 50-100 nm size¹⁸.

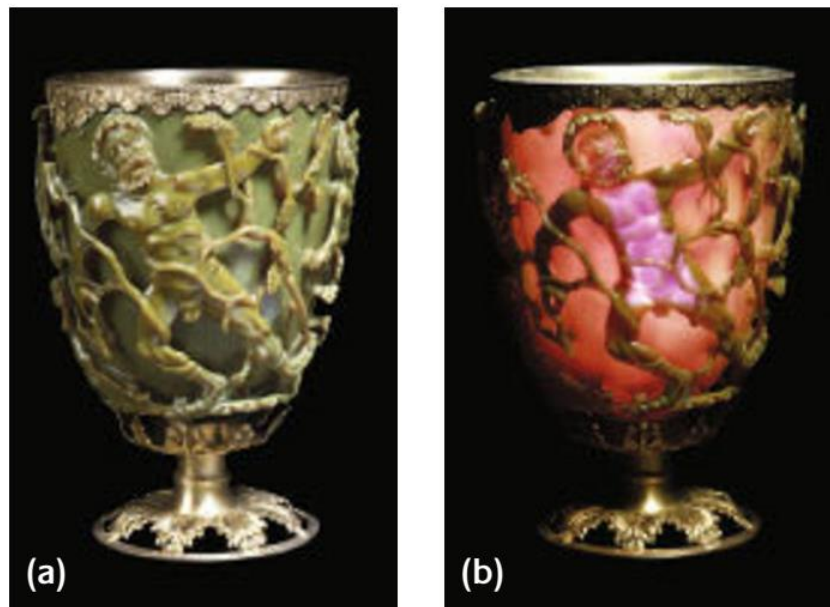


Figure 2. The Lycurgus Cup 1958,1202.1 in reflected (a) and transmitted (b) light¹⁸. Department of Prehistory and Europe, The British Museum. © The Trustees of the British Museum. Reproduced (adapted) from¹⁸. License: CC BY-NC 2.0

Researchers' interest in the synthesis of gold-silver alloy nanoparticles dates back to the 1970s^{19, 20}. Nowadays, the synthesis of gold-silver alloy nanoparticles is considered as a relatively mature research field. Among the methods to prepare gold-silver alloy nanoparticles, the co-reduction of gold and silver precursors by chemical reductant is the most frequently used one. This method has been performed in organic solution²¹ and aqueous solution²², where the composition and size of alloy nanoparticles can be controlled by varying both the precursor ratios and the amounts of reductant.

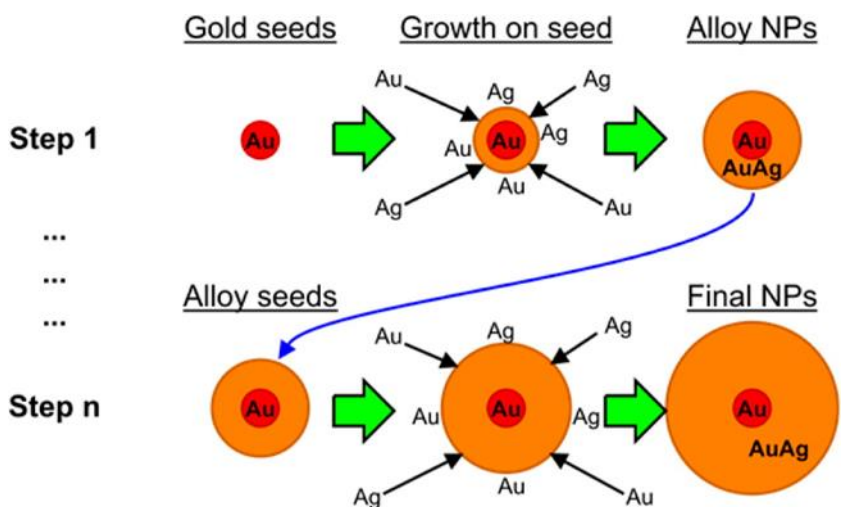


Figure 3. Schematic of the multistep seeded growth synthesis of gold-silver alloy nanoparticles²³. Reprinted with permission from²³. Copyright (2015) American Chemical Society.

According to the LaMer mechanism^{24, 25}, the growth process of nanoparticles involves two different periods, the size focusing period and Ostwald ripening period. In size focusing period, the mean diameters of the nanoparticles increases rapidly and the size distribution becomes narrower while the growth rates declines sharply and the size distributions broadens in Ostwald ripening period²⁶. The switching point of these two different periods depends on the ratio of metal precursors to monomers (reacted species readily to nucleate) concentration: the size focusing period is favored at low ratio while the Ostwald ripening period is favored at high ratio. Since the concentration of monomers decreases by nanoparticle growth, multiple seeded-growth steps, where the precursors to monomers ratio is low, are required to form monodisperse large size gold-silver alloy nanoparticle with diameter above 50 nm. With the employment of seeded growth and co-

reduction, it is more readily to prepare large gold-silver alloy nanoparticles with small size distribution. Gold nanoparticle has been reported to act as a starting seed to grow the thick alloy shell from the co-reduction of gold and silver precursors²³, where the resulting nanoparticles are used as seeds for the subsequent growth step and this process is repeated until the desired size is reached (Figure 3). In addition to gold nanoparticle, our research work demonstrates that gold-silver alloy nanoparticle can work as starting seed in the preparation of monodisperse large gold-silver alloy nanoparticles, which enables better control over the composition and will be described in detail in Chapter Two. It is also worthy to note that core-shell gold/silver nanoparticle can be converted into gold-silver alloy nanoparticles by annealing at high temperature²⁷(Figure 4), which is similar with seeded growth process of Figure 3.

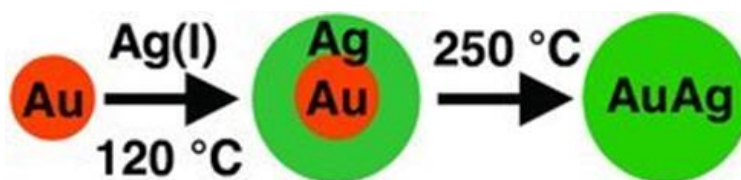


Figure 4. The synthesis of Au(core)/Ag(shell) NPs and their conversion to AuAg alloy NPs through annealing²⁷. Reprinted with permission from²⁷. Copyright (2011) WILEY VCH.

In addition to the conventional chemical reduction method, novel methods such as galvanic replacement²⁸, sonochemical technique²⁹, and laser ablation^{30, 31} are reported for the synthesis of gold-silver alloy nanoparticles. Galvanic replacement makes use of different redox potentials of varied metal/metal ion couples. As metal ions with higher

standard redox potential may receive electrons from metal nanoparticles with lower redox potential, silver nanoparticles are usually the sacrificial template, given that the standard electrode potential of $\text{Ag}^+_{(\text{aq})}/\text{Ag}_{(\text{s})}$ is 0.80 V and the one of $[\text{AuCl}_4]^-/\text{Au}_{(\text{s})}$ is 0.93 V³². It has been reported²⁸ that monodisperse Ag-Au alloy nanoparticles from 6 nm to 11 nm with only 0.5 nm deviation are prepared by the replacement reaction between Ag nanoparticles and HAuCl_4 in the absence of reductant. In sonochemical technique, the high frequency sound (from 20 kHz to several MHz) is transmitted through a medium as a pressure wave and induces a vibrational motion of the molecules, which could deliver energy into the reaction mixture leading to local temperature change from 1900 to 5200 K, pressures change about 10^3 atm with heating/cooling rates above 10^8 K·s⁻¹ in room temperature lab²⁹. Laser ablation in liquids is probably the most versatile method for fast production of nanoalloys with arbitrary composition³⁰. As an energy source that drives the reactant molecules in ground state to go across the energy barrier, laser ablation facilitates the reduction of metal ions by high energy electrons and radicals produced in situ through the ionization and excitation of solvent molecules by irradiation energy³¹. As is shown in Figure 5, near-monodispersed gold-silver alloy nanoparticles are synthesized by high intensity laser irradiation of metal ions in hexane without other reductants with different gold-silver ratios and the average size of 2–5 nm³¹. Although gold-silver alloy nanoparticles with 20% Au and diameter as 105 ± 28 nm has been prepared by laser ablation³³, more efforts are required to improve this synthesis method to achieve better control over the alloy nanoparticles' size and composition.

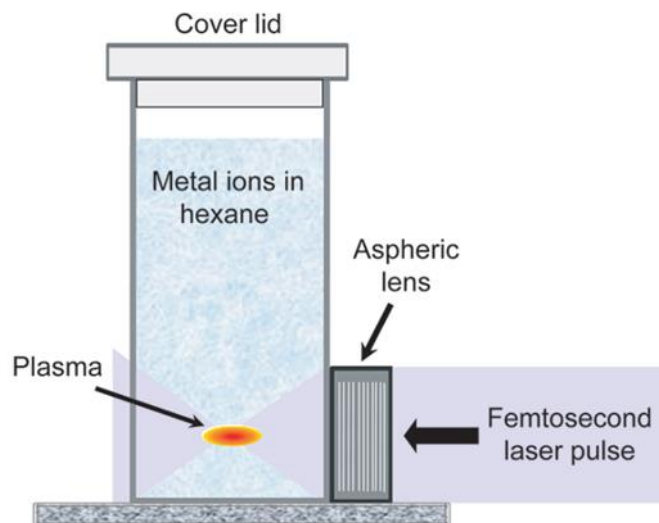


Figure 5. Sketch of the experimental setup³¹. Reprinted with permission from³¹. Copyright (2011) American Chemical Society.

1.3 Applications of gold-silver alloy nanoparticles

Gold-silver alloy nanoparticle has remained one of the trending research topics over several decades because of its tunable plasmonic property by controlling nanoparticle size, shape and composition. As is presented in Figure 6¹⁷, the localized surface plasmon resonance wavelengths from 390 nm to 530 nm are attainable in the range of diameters from 5 nm to 50 nm and gold fractions from 0 to 1. The tunable plasmon resonance makes gold-silver alloy nanoparticles a versatile candidate in localized surface plasmon related applications such as dark-field imaging³⁴, plasmon-enhanced fluorescence³⁵ and photothermal effect³⁶.

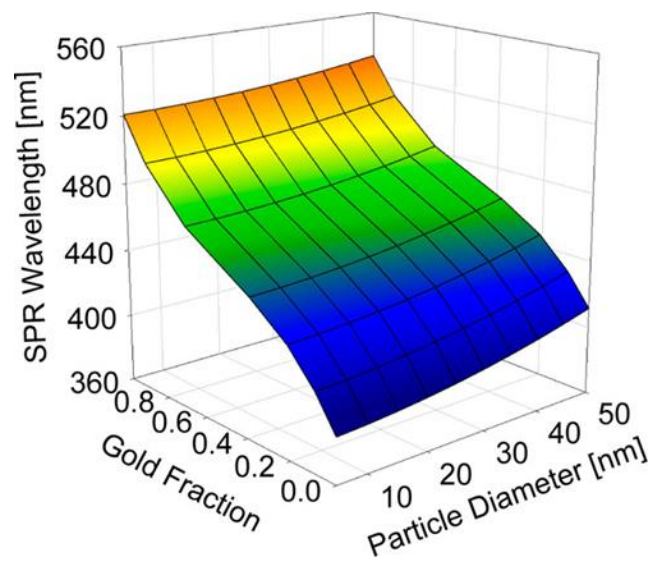


Figure 6. Mesh plot of the SPR wavelength of $\text{Au}_x\text{Ag}_{(1-x)}$ alloy nanoparticles as a function of gold content and particle diameter predicted by Mie theory¹⁷. Reprinted with permission from¹⁷. Copyright (2013) American Chemical Society.

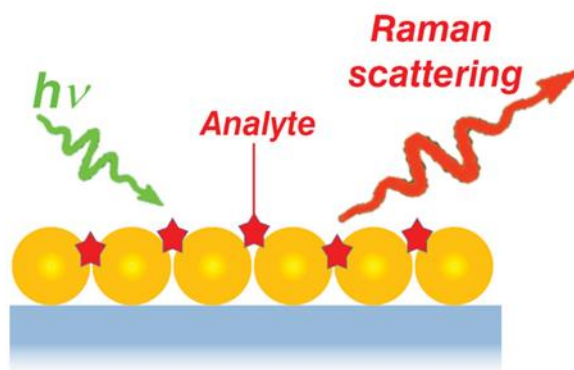


Figure 7. Schematic for analyte molecules Raman scattering enhanced by plasmonic nanoparticles³. Reprinted with permission from³. Copyright (2017) IOP Publishing.

Among the plasmon related applications, gold-silver alloy nanoparticles have been commonly used in surface enhancement Raman spectroscopy (SERS). SERS is a

surface sensitive technique to enhance Raman scattering by molecules adsorbed on metal surface or molecules in the vicinity of plasmonic nanostructures³⁷(Figure 7). For SERS substrate fabricated from plasmonic nanostructures, both chemical and electromagnetic enhancement mechanisms are well accepted as key contributors to SERS phenomenon³⁸. It has been demonstrated that SERS signal is measured in the complicated matrix such as urine or blood³⁸. Silver is considered the most useful for SERS enhancement in term of sensitivity^{38, 39} but silver is more likely to undergo oxidation, which leads to a significant decrease of SERS activity over time⁴⁰. The incorporation of silver and gold into alloy NPs could reduce the toxicity by minimizing the release of silver ions as compared to pure silver nanoparticles⁴¹⁻⁴⁴, making gold-silver alloy nanoparticle more stable for bio-imaging applications over time³⁹. Besides, computational work and experimental results have shown that the SERS properties of gold and silver nanoparticles highly depend on their shape⁴⁵. Gold-silver alloy nanostructures with sharp tips or edges such as nanowires³⁸, nanoboxes⁴⁶ and nanodendrites⁴⁷ enable strong SERS performance because there will be more hot spots and more molecules will be absorbed on the nanoparticle surface as the surface area of these nanostructures increases.

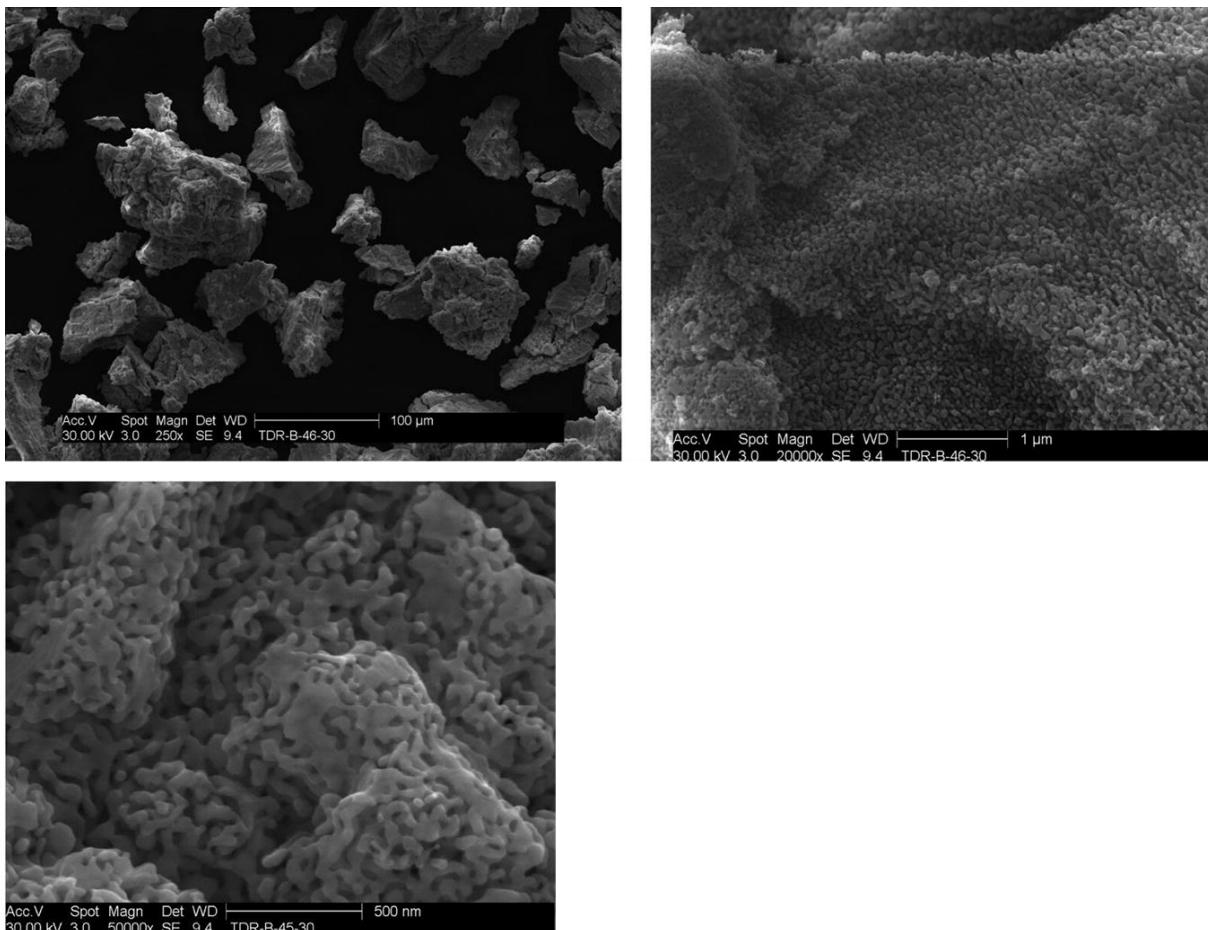


Figure 8. SEM (scanning electron microscope) images of Ag₂Au₉₈ catalyst, where the size of the gold-silver crystallites is close to 8 nm estimated the X-ray diffraction peaks⁴⁸. Reprinted with permission from⁴⁸. Copyright (2014) Elsevier.

Another important application of gold-silver alloy nanoparticles is acting as catalysts. Gold nanoparticles play an important catalyst role in several oxidation reactions though the mechanism is still in debate⁴⁹. An option to enhance the catalytic activity of gold nanoparticles is to search for a metallic element that can be alloyed with gold in nanoscale and has more affinity to oxygen, which is silver. Ag and Au have nearly identical lattice constants (0.408 nm for Au and 0.409 nm for Ag), which could lead to alloy

formation under certain synthetic conditions⁵⁰. It has been reported that high catalytic activity and selectivity towards the oxidation reactions of H₂ and CO are achieved by Ag-Au nanoalloys⁴⁸ (Figure 8). Compared with monometallic Au or Ag catalysts, the alloy catalysts exhibited much higher activity at low temperature for both CO oxidation and H₂ oxidation⁴⁸. Both the reaction rates of H₂ oxidation and CO oxidation have positive correlations with silver concentration (from 0% to 6%), which may be correlated with the number of surface sites constituted of adjacent Ag atoms that are required for dissociative oxygen adsorption.

1.4 Conclusion

Based on its unique tunable plasmonic properties, gold-silver alloy nanoparticles have attracted many research interests over several decades. Although the synthesis of gold-silver alloy nanoparticles is considered as a relatively mature research field, more efforts are required to develop the synthesis methods that have better control of alloy nanoparticles' size, shape and composition, especially for non-spherical nanoparticles, which will pave the way for the following properties and application studies. In addition, it is anticipated that gold-silver alloy nanoparticles will be applied for more and more bio-applications in the future with the rapid development of biomedicine nowadays. We hope the knowledge presented in this chapter will be beneficial for our readers to have better understandings of the following three research chapters.

1.5 Reference

1. Maier, S. A., *Plasmonics: fundamentals and applications*. Springer: 2007; Vol. 1.
2. Kittel, C.; McEuen, P., *Kittel's Introduction to Solid State Physics*. John Wiley & Sons: 2018.
3. Amendola, V.; Pilot, R.; Frascioni, M.; Maragò, O. M.; Iatì, M. A., Surface plasmon resonance in gold nanoparticles: a review. *Journal of Physics: Condensed Matter* **2017**, *29* (20), 203002.
4. Moores, A.; Goettmann, F., The plasmon band in noble metal nanoparticles: an introduction to theory and applications. *New Journal of Chemistry* **2006**, *30* (8), 1121-1132.
5. Khlebtsov, N. G.; Dykman, L. A., Optical properties and biomedical applications of plasmonic nanoparticles. *Journal of Quantitative Spectroscopy and Radiative Transfer* **2010**, *111* (1), 1-35.
6. Pissuwan, D.; Cortie, C. H.; Valenzuela, S. M.; Cortie, M. B., Functionalised gold nanoparticles for controlling pathogenic bacteria. *Trends in biotechnology* **2010**, *28* (4), 207-213.
7. Sperling, R. A.; Gil, P. R.; Zhang, F.; Zanella, M.; Parak, W. J., Biological applications of gold nanoparticles. *Chemical Society Reviews* **2008**, *37* (9), 1896-1908.
8. Kelly, K. L.; Coronado, E.; Zhao, L. L.; Schatz, G. C., The optical properties of metal nanoparticles: the influence of size, shape, and dielectric environment. *The Journal of Physical Chemistry B*: 2003; Vol. 107, pp 668-677.
9. Mayer, K. M.; Hafner, J. H., Localized surface plasmon resonance sensors. *Chemical reviews* **2011**, *111* (6), 3828-3857.
10. Liebsch, A., Surface-plasmon dispersion and size dependence of Mie resonance: silver versus simple metals. *Physical Review B* **1993**, *48* (15), 11317.
11. Grady, N. K.; Halas, N. J.; Nordlander, P., Influence of dielectric function properties on the optical response of plasmon resonant metallic nanoparticles. *Chemical Physics Letters* **2004**, *399* (1-3), 167-171.
12. Link, S.; Wang, Z. L.; El-Sayed, M., Alloy formation of gold– silver nanoparticles and the dependence of the plasmon absorption on their composition. *The Journal of Physical Chemistry B* **1999**, *103* (18), 3529-3533.
13. Sau, T. K.; Rogach, A. L.; Jäckel, F.; Klar, T. A.; Feldmann, J., Properties and applications of colloidal nonspherical noble metal nanoparticles. *Advanced Materials* **2010**, *22* (16), 1805-1825.
14. Zhou, J.; Yang, T.; He, W.; Pan, Z. Y.; Huang, C. Z., A galvanic exchange process visualized on single silver nanoparticles via dark-field microscopy imaging. *Nanoscale* **2018**, *10* (26), 12805-12812.
15. Taniguchi, K.; Jin, X.; Yamaguchi, K.; Nozaki, K.; Mizuno, N., Versatile routes for synthesis of diarylamines through acceptorless dehydrogenative aromatization catalysis over supported gold–palladium bimetallic nanoparticles. *Chemical science* **2017**, *8* (3), 2131-2142.
16. Stamenkovic, V. R.; Mun, B. S.; Arenz, M.; Mayrhofer, K. J.; Lucas, C. A.; Wang, G.; Ross, P. N.; Markovic, N. M., Trends in electrocatalysis on extended and nanoscale Pt-bimetallic alloy surfaces. *Nature materials* **2007**, *6* (3), 241-247.

17. Verbruggen, S. W.; Keulemans, M.; Martens, J. A.; Lenaerts, S., Predicting the surface plasmon resonance wavelength of gold–silver alloy nanoparticles. *The Journal of Physical Chemistry C* **2013**, *117* (37), 19142-19145.
18. Freestone, I.; Meeks, N.; Sax, M.; Higgitt, C., The Lycurgus cup—a roman nanotechnology. *Gold bulletin* **2007**, *40* (4), 270-277.
19. Cortie, M. B.; McDonagh, A. M., Synthesis and optical properties of hybrid and alloy plasmonic nanoparticles. *Chemical reviews* **2011**, *111* (6), 3713-35.
20. Papavassiliou, G. C., Surface plasmons in small Au-Ag alloy particles. *Journal of Physics F: Metal Physics* **1976**, *6* (4), L103.
21. Liu, S.; Chen, G.; Prasad, P. N.; Swihart, M. T., Synthesis of monodisperse Au, Ag, and Au–Ag alloy nanoparticles with tunable size and surface plasmon resonance frequency. *Chemistry of Materials* **2011**, *23* (18), 4098-4101.
22. Ristig, S.; Prymak, O.; Loza, K.; Gocyla, M.; Meyer-Zaika, W.; Heggen, M.; Raabe, D.; Epple, M., Nanostructure of wet-chemically prepared, polymer-stabilized silver–gold nanoalloys (6 nm) over the entire composition range. *Journal of Materials Chemistry B* **2015**, *3* (23), 4654-4662.
23. Rioux, D.; Meunier, M., Seeded Growth Synthesis of Composition and Size-Controlled Gold–Silver Alloy Nanoparticles. *The Journal of Physical Chemistry C* **2015**, *119* (23), 13160-13168.
24. LaMer, V. K.; Dinegar, R. H., Theory, production and mechanism of formation of monodispersed hydrosols. *Journal of the american chemical society* **1950**, *72* (11), 4847-4854.
25. Reiss, H., The growth of uniform colloidal dispersions. *The Journal of Chemical Physics* **1951**, *19* (4), 482-487.
26. Bastús, N. G.; Comenge, J.; Puentes, V., Kinetically controlled seeded growth synthesis of citrate-stabilized gold nanoparticles of up to 200 nm: size focusing versus Ostwald ripening. *Langmuir* **2011**, *27* (17), 11098-11105.
27. Shore, M. S.; Wang, J.; Johnston-Peck, A. C.; Oldenburg, A. L.; Tracy, J. B., Synthesis of Au (Core)/Ag (Shell) nanoparticles and their conversion to AuAg alloy nanoparticles. *Small* **2011**, *7* (2), 230-234.
28. Zhang, Q.; Xie, J.; Liang, J.; Lee, J. Y., Synthesis of Monodisperse Ag₂ Au Alloy Nanoparticles with Independently Tunable Morphology, Composition, Size, and Surface Chemistry and Their 3-D Superlattices. *Advanced Functional Materials* **2009**, *19* (9), 1387-1398.
29. Radziuk, D.; Shchukin, D.; Möhwald, H., Sonochemical design of engineered gold– silver nanoparticles. *The Journal of Physical Chemistry C* **2008**, *112* (7), 2462-2468.
30. Papagiannouli, I.; Aloukos, P.; Rioux, D.; Meunier, M.; Couris, S., Effect of the Composition on the Nonlinear Optical Response of Au x Ag_{1-x} Nano-Alloys. *The Journal of Physical Chemistry C* **2015**, *119* (12), 6861-6872.
31. Herbani, Y.; Nakamura, T.; Sato, S., Synthesis of near-monodispersed Au–Ag nanoalloys by high intensity laser irradiation of metal ions in hexane. *The Journal of Physical Chemistry C* **2011**, *115* (44), 21592-21598.
32. Haynes, W. M.; Lide, D. R.; Bruno, T. J., *CRC handbook of chemistry and physics*. CRC press: 2016.

33. Al-Zubeidi, A.; Stein, F.; Flatebo, C.; Rehbock, C.; Hosseini Jebeli, S. A.; Landes, C. F.; Barcikowski, S.; Link, S., Single-Particle Hyperspectral Imaging Reveals Kinetics of Silver Ion Leaching from Alloy Nanoparticles. *ACS nano* **2021**, *15* (5), 8363-8375.
34. Patskovsky, S.; Bergeron, E.; Rioux, D.; Simard, M.; Meunier, M., Hyperspectral reflected light microscopy of plasmonic Au/Ag alloy nanoparticles incubated as multiplex chromatic biomarkers with cancer cells. *Analyst* **2014**, *139* (20), 5247-5253.
35. Stranik, O.; Nooney, R.; McDonagh, C.; MacCraith, B. D., Optimization of nanoparticle size for plasmonic enhancement of fluorescence. *Plasmonics* **2007**, *2* (1), 15-22.
36. Borah, R.; Verbruggen, S. W., Silver-gold bimetallic alloy versus core-shell nanoparticles: Implications for plasmonic enhancement and photothermal applications. *The Journal of Physical Chemistry C* **2020**, *124* (22), 12081-12094.
37. Xu, X.; Li, H.; Hasan, D.; Ruoff, R. S.; Wang, A. X.; Fan, D., Near-field enhanced plasmonic-magnetic bifunctional nanotubes for single cell bioanalysis. *Advanced Functional Materials* **2013**, *23* (35), 4332-4338.
38. Wiriyakun, N.; Pankhluab, K.; Boonrungsiman, S.; Laocharoensuk, R., Site-selective controlled dealloying process of gold-silver nanowire array: a simple approach towards long-term stability and sensitivity improvement of SERS substrate. *Scientific reports* **2016**, *6* (1), 1-11.
39. Li, H.; Liu, H.; Qin, Y.; Mu, Y.; Fang, X.; Zhai, T.; Zhang, X., Gold-Stabilized Gold-Silver Alloy Nanostructures as High-Performance SERS Substrate. *Plasmonics* **2020**, *15* (6), 2027-2032.
40. Ma, L.; Huang, Y.; Hou, M.; Xie, Z.; Zhang, Z., Silver nanorods wrapped with ultrathin Al₂O₃ layers exhibiting excellent SERS sensitivity and outstanding SERS stability. *Scientific reports* **2015**, *5* (1), 1-9.
41. Sotiriou, G. A.; Etterlin, G. D.; Spyrogianni, A.; Krumeich, F.; Leroux, J.-C.; Pratsinis, S. E., Plasmonic biocompatible silver-gold alloyed nanoparticles. *Chemical Communications* **2014**, *50* (88), 13559-13562.
42. Tiedemann, D.; Taylor, U.; Rehbock, C.; Jakobi, J.; Klein, S.; Kues, W. A.; Barcikowski, S.; Rath, D., Reprotoxicity of gold, silver, and gold-silver alloy nanoparticles on mammalian gametes. *Analyst* **2014**, *139* (5), 931-942.
43. Ristig, S.; Chernousova, S.; Meyer-Zaika, W.; Epple, M., Synthesis, characterization and in vitro effects of 7 nm alloyed silver-gold nanoparticles. *Beilstein journal of nanotechnology* **2015**, *6* (1), 1212-1220.
44. Mahl, D.; Diendorf, J.; Ristig, S.; Greulich, C.; Li, Z.-A.; Farle, M.; Köller, M.; Epple, M., Silver, gold, and alloyed silver-gold nanoparticles: characterization and comparative cell-biologic action. *Journal of Nanoparticle Research* **2012**, *14* (10), 1153.
45. Shen, X. S.; Wang, G. Z.; Hong, X.; Zhu, W., Nanospheres of silver nanoparticles: agglomeration, surface morphology control and application as SERS substrates. *Physical Chemistry Chemical Physics* **2009**, *11* (34), 7450-7454.
46. Li, J.; Wang, J.; Grewal, Y. S.; Howard, C. B.; Raftery, L. J.; Mahler, S.; Wang, Y.; Trau, M., Multiplexed SERS detection of soluble cancer protein biomarkers with gold-silver alloy nanoboxes and nanoyeast single-chain variable fragments. *Analytical chemistry* **2018**, *90* (17), 10377-10384.
47. da Silva, A. G.; de Souza, M. L.; Rodrigues, T. S.; Alves, R. S.; Temperini, M. L.; Camargo, P. H., Rapid synthesis of hollow Ag-Au nanodendrites in 15 seconds by combining

galvanic replacement and precursor reduction reactions. *Chemistry–A European Journal* **2014**, *20* (46), 15040-15046.

48. Déronzier, T.; Morfin, F.; Lomello, M.; Rousset, J.-L., Catalysis on nanoporous gold–silver systems: Synergistic effects toward oxidation reactions and influence of the surface composition. *Journal of catalysis* **2014**, *311*, 221-229.

49. Hvolbæk, B.; Janssens, T. V.; Clausen, B. S.; Falsig, H.; Christensen, C. H.; Nørskov, J. K., Catalytic activity of Au nanoparticles. *Nano today* **2007**, *2* (4), 14-18.

50. Li, T.; Albee, B.; Alemayehu, M.; Diaz, R.; Ingham, L.; Kamal, S.; Rodriguez, M.; Bishnoi, S. W., Comparative toxicity study of Ag, Au, and Ag–Au bimetallic nanoparticles on *Daphnia magna*. *Analytical and bioanalytical chemistry* **2010**, *398* (2), 689-700.

Chapter 2. Two-step synthesis of gold-silver alloy nanoparticles via the combination of seeded growth and citrate co-reduction

2.1 Introduction

Noble metal nanoparticles (NPs) are one of the most well-studied nanomaterials because of their well-controlled preparation¹⁻³ and their attractive catalytic⁴⁻⁶ and optical properties⁷⁻¹⁰, which originate from their plasmonic properties. Plasmons are collective oscillations of free electrons under irradiation. Among plasmonic nanoparticles, most research has been focused on gold and silver because they are well suited for sustaining a plasmon resonance in the visible region of the spectrum¹¹. Gold exhibits an intrinsically weaker plasmonic resonance than silver because silver has smaller losses in the UV and visible region of the spectrum^{12, 13}. However, gold is often preferred to silver for its better biocompatibility and chemical stability. Ag NPs are toxic in a liquid environment over time due to the surface oxidation and dissolution of silver ions^{14, 15}. However, the incorporation of silver and gold into alloy NPs could reduce the toxicity by minimizing the release of silver ions as compared to pure silver nanoparticles¹⁶⁻¹⁹ while enhancing the plasmonic resonance of the nanoparticles. Ag and Au have nearly identical lattice constants (0.408 nm for Au and 0.409 nm for Ag), which could lead to alloy formation under some synthetic conditions²⁰. To date, most of the plasmonic research focuses on sub-10 nm NPs²¹⁻²⁷. However, since the plasmonic band detected in the optical extinction spectra originates from the sum of scattered and absorbed photons with a proportion strongly dependent on NPs' size¹³, plasmonic NPs with diameters larger than 30 nm exhibiting greater scattering are generally required for bio-imaging applications such as Rayleigh scattering²⁸⁻³²,

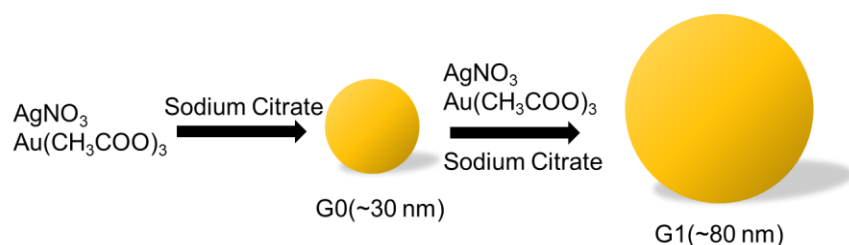
surface enhanced Raman spectroscopy³³⁻³⁵, plasmon enhanced fluorescence³⁶⁻⁴⁰ and optical trapping⁴¹⁻⁴³. The plasmonic characteristics of noble metal NPs are highly dependent on their size, composition and shape, which could be controlled by different synthetic methods. The tuning of composition and particle size of gold-silver alloy NPs could provide a wide range of plasmon resonance wavelengths for application optimization⁴⁴.

The formation process of nanoparticles can be explained by the commonly accepted LaMer model^{45, 46} separating nucleation and growth: nuclei are generated at the same time due to homogeneous nucleation and subsequently grow without additional nucleation⁴⁷. As a consequence, many nucleation events lead to many small NPs, and few nucleation events to fewer and larger NPs, which rationalizes the “seeded-growth” strategy by suppressing further nucleation⁴⁷. Synthesis of gold-silver alloy NPs has been reported as early as 1999⁴⁸ based on citrate co-reduction with diameters around 20 nm. Currently, citrate co-reduction of gold and silver precursors remains one of the most common methods to produce gold-silver alloy NPs^{49, 50}. Citrate reduction of chloroauric acid in aqueous solution, also known as the Turkevich⁵¹ method, is the most commonly employed method to synthesize gold nanoparticles. Following the Turkevich method, it is possible to control the diameters of gold NPs from 5 to 150 nm by simply varying the reaction conditions, but the prepared gold NPs are of poor quality (size and diameter distribution) with irregular shapes¹. Bastús et al.¹ reported a general synthesis route to prepare large (around 180 nm), uniform quasi-spherical and monodisperse Au NPs with the combination of citrate reduction of chloroauric acid and seeded growth, which is the major inspiration of our study. Meanwhile, there have been a few recent advancements

in the preparation of gold-silver alloy nanoparticles with diameters larger than 30 nm by chemical reduction^{50, 52-54} or laser ablation⁵⁵. However, these reports did not demonstrate good control of the composition and diameters of the resulting alloy nanoparticles, or selected chloroauric acid as the gold precursor, which may result in the formation of silver chloride precipitate. As the solubility product of AgCl is fairly small (1.6×10^{-10}), the concentration of silver precursors and large-scale synthesis will be limited in the future. Many efforts have been reported to minimize the effect of chloride from the chloroauric acid precursor⁵⁶⁻⁵⁸, but a clear-cut answer is the use of chloride-free precursor, gold acetate.

Here, we describe a novel synthesis method for large gold-silver alloy NPs whose diameters are ~ 80 nm using gold acetate and silver nitrate as precursors and sodium citrate as a mild reductant in aqueous solution. This method relies on the joint efforts of citrate co-reduction and a seeded growth strategy in two steps (Scheme 1). Step one is to synthesize the gold-silver alloy seeds (G0) with diameters ~ 30 nm by citrate co-reduction of gold acetate and silver nitrate. Next, the seeds grow into large alloy nanoparticles (G1) with diameters ~ 80 nm by the combination of seeded growth and citrate co-reduction of gold and silver precursors. To our knowledge, it is the first to prepare gold-silver alloy nanoparticles with diameter ~ 80 nm using gold acetate as the gold precursors. Using acetate as the precursor enables better control over silver content than with the more common chloroauric acid, since silver acetate is soluble in water, while silver chloride is not. The prepared gold-silver alloy seeds and large NPs are monodispersed, uniformly quasi-spherical and highly crystalline. The size, shape and composition of the gold-silver alloy NPs were investigated by transmission electron

microscopy (TEM) and energy-dispersive X-ray spectroscopy (EDAX) mapping. EDAX mapping shows that both gold and silver are distributed uniformly within the cores of all synthesized gold-silver alloy NPs. Interestingly, a silver-rich surface appears in all synthesized alloy nanoparticles, including NPs with only 25% silver content. As expected, this silver enriched surface layer is thicker and more prominent in 75% silver NPs when compared to the other alloy NPs. In addition, we demonstrate that while this silver surface layer does not appear as a separate plasmonic feature, the plasmonic band of these gold-silver alloy NPs can be tuned by controlling the size and composition of the alloy NPs.



Scheme 1 Schematic illustration of synthesis of Au-Ag alloy nanoparticles using seeded growth method

2.2 Experimental

2.2.1 Materials

All glassware were washed by aqua regia and nitric acid before use. All chemicals were used without further purification. Gold(III) acetate (99.9%, Alfa Aesar), silver nitrate (>99%, Sigma-Aldrich) and sodium citrate (Sigma-Aldrich). Deionized (DI) water (>18 $\text{M}\Omega\cdot\text{cm}$) was used and obtained using Barnstead Diamond TII (Thermo Fisher) purification system. Centrifugations were performed with a SORVALL RC 6 PLUS centrifuge (Thermo Fisher Scientific, Waltham, MA) using a SH-3000 swinging rotor.

2.2.2 Synthesis of gold-silver alloy seeds nanoparticles

The synthesis of gold-silver alloy seeds nanoparticles was achieved using a modified Turkevich approach⁵¹. Briefly, gold acetate and silver nitrate (6 μmol in total) were added to 50 mL of DI water in a 100 mL round bottom flask with 25 mg of sodium citrate. The solution was heated by water bath from room temperature to 75 degrees Celsius with stirring. Keep stirring and maintain the temperature at 75 degrees for three hours to ensure complete reduction of gold and silver ions. The solution would become transparent and its color gradually changed into yellow-green (25% Au), yellow (50% Au), yellow-red (75% Au) and ruby red (100% Au), respectively. The Au content in resultant alloy nanoparticles was controlled by adjusting the amount of gold precursor, gold acetate. Thus, by increasing the amount of gold acetate from 1.5 μmol to 3 μmol , 4.5 μmol and 6 μmol , 25% Au, 50% Au, 75% Au alloy seeds and pure gold nanoparticles could be prepared.

2.23 Synthesis of pure silver nanoparticles

As silver nitrate could not be reduced by sodium citrate solely, the synthesis method of pure silver nanoparticles was adopted from literature² and it is based on the reduction of silver nitrate by a combination of two reductant: sodium citrate and tannic acid. Briefly, a 100 mL volume solution containing sodium citrate (5 mM) and tannic acid (0.25 mM) was prepared and heated under vigorous stirring with a condenser. After boiling had commenced, 1 mL of silver nitrate (25 mM) was injected into this solution. The color of solution changed into green-yellow within a few seconds. The resultant pure silver nanoparticles were purified by centrifugation (4500 rpm for 30 minutes) and further redispersed in DI water.

2.24 Synthesis of gold silver alloy seeded-growth nanoparticles

Gold-silver alloy seeds nanoparticles were synthesized following the above-described protocol. 10 mL of resultant gold-silver alloy seeds were purified by centrifugation (4500 rpm for 30 minutes) to remove the excess of unreacted gold and silver ions and sodium citrate, and then were redispersed in 50 mL DI water. Gold acetate and silver nitrate (5 μ mol in total) were added to the solution in a 100 mL round bottom flask with 12.5 mg sodium citrate. The solution was heated by water bath from room temperature to 90 degrees Celsius with stirring. Keep stirring and maintain the temperature at 90 degrees for one hour to ensure complete reduction of gold and silver ions. The solution would gradually become more yellow-green (25% Au), yellow (50% Au), yellow-red (75% Au), respectively.

2.25 UV-vis, TEM and EDAX characterization

UV-visible extinction spectra in the 200-800 nm region were collected using a Cary 100 Bio instrument. The size, morphology and size distribution were characterized by TEM (Philips CM200 TEM) and high-resolution TEM (Thermo Scientific Talos F200X G2 S/TEM). Samples were plated on 400 mesh carbon-coated copper grids (Ted Pella) overnight before characterization. Images were collected using CM200 and Talos at 200 kV. Analysis of TEM images was carried out using ImageJ 1.53i (Wayne Rasband, National Institutes of Health, USA). EDAX measurements were conducted by Talos STEM (Scanning Transmission Electron Microscopy) with HAADF (high-angle annular dark field) detectors.

2.3 Results and Discussion

While sodium citrate is commonly used as both a reducing and a stabilizing agent in the synthesis of gold nanoparticles, there are very few reported cases for the synthesis of silver nanoparticles with sodium citrate because of silver ions' lower reduction potential. The challenge to produce monodisperse and uniform composition gold-silver alloy nanoparticles lies with the different reduction potentials of gold and silver. Alloy formation within the nanoparticle is indicated by the presence of only one plasmonic peak in optical extinction spectra⁴⁸. Two plasmonic peaks are expected for distinct core-shell nanostructures^{25, 59, 60}. The optical spectra of both the gold-silver alloy seeds and the seeded-grown nanoparticles in Figure 1 indicate alloy formation rather than core-shell nanostructures. Figure 1(a) shows the UV-Vis extinction spectra of several gold-silver alloy nanoparticles (seeds) with varying gold content. All nanoparticle seeds exhibit a single band, with their peak max ranging from 416 nm (for pure silver NPs) to 530 nm (for pure gold NPs). A linear relationship is achieved as expected for alloy nanostructures with increasing gold content (Figure 1, inset). The λ_{\max} for the plasmonic peaks of seeded-grown alloy nanoparticles in Figure 1(b) lie between reported pure silver² (451 nm) and gold¹ (546 nm) nanoparticles' with comparable diameters and red-shifts with higher gold in composition of alloy nanoparticles.

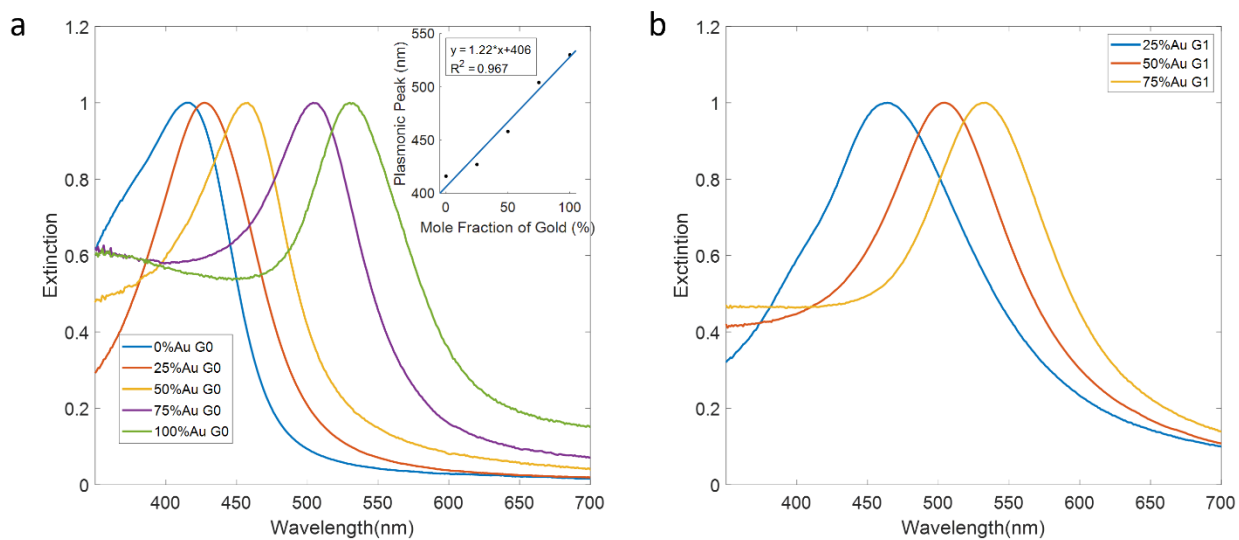


Figure 1. UV-vis spectra of Au–Ag alloy nanoparticles. (a) seed alloy nanoparticles(G0). (inset: plot of the wavelength corresponding to the plasmonic band as a function of gold mole fraction for Au–Ag alloy nanoparticles) (b) seeded-grown alloy nanoparticles(G1).

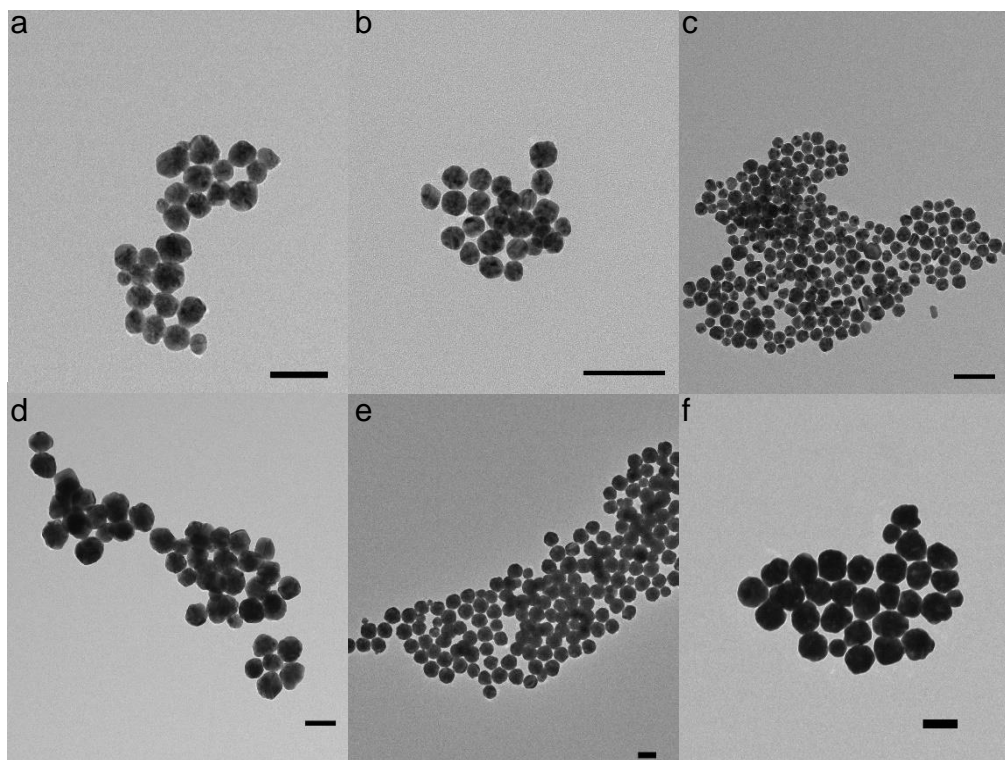


Figure 2. TEM images of Au-Ag alloy nanoparticles samples. (a)25%Au G0 nanoparticles.

(b)50%Au G0 nanoparticles. (c)75%Au G0 nanoparticles. (d)25%Au G1 nanoparticles. (e)50%Au G1 nanoparticles. (f)75%Au G1 nanoparticles. Scale bar is 100 nm for all images.

TEM images (Figure 2) reveal a uniform size dispersion for all nanoparticles samples. The seed alloy nanoparticles (G0) have diameters close to 30 nm except for 25%Au G0, which has a diameter of 42 nm. In addition, the size distribution of 25%Au G0 is also wider than the other two seed samples. After seeded growth, the different G1 alloy nanoparticles also have a similar size in this case around 80 nm. All samples show a quasi-spherical shape that becomes less spherical as the content of silver increases, which may result from the increased mobility of silver atoms⁶¹. The mean diameter distributions, based on more than 100 nanoparticles, are narrow as shown in Figure 4 and Table 1. More details of the morphology and crystallinity of nanoparticles are shown in their high-resolution-TEM(HRTEM) images (Figure 3). HRTEM images also show a high degree of crystallinity and well-defined lattice fringes. The interplanar distance measured from the adjacent lattice fringes is about 0.24 nm for the six different gold-silver alloy nanoparticles, which indicates (111) planes of face-centered cubic (fcc) gold or silver.

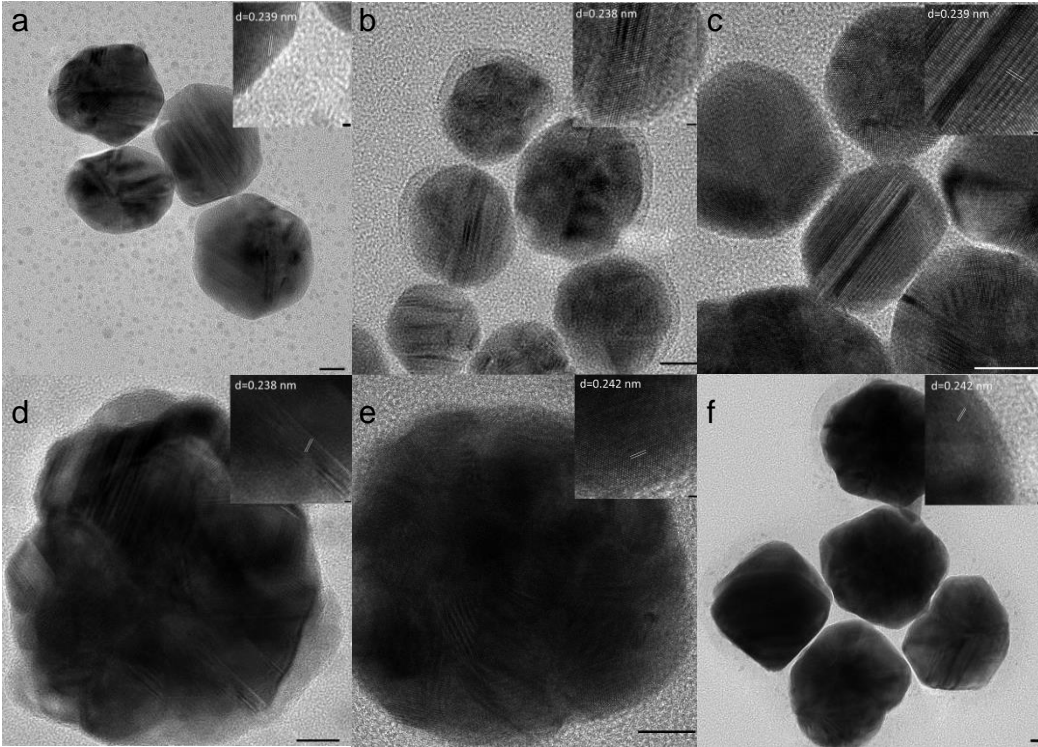


Figure 3. High resolution TEM images of Au-Ag alloy nanoparticles samples.

(a)25%Au G0 nanoparticles. (b)50%Au G0 nanoparticles. (c)75%Au G0 nanoparticles.

(d)25%Au G1 nanoparticles. (e)50%Au G1 nanoparticles. (f)75%Au G1 nanoparticles.

Scale bar is 10 nm and 1 nm (inset) for all images.

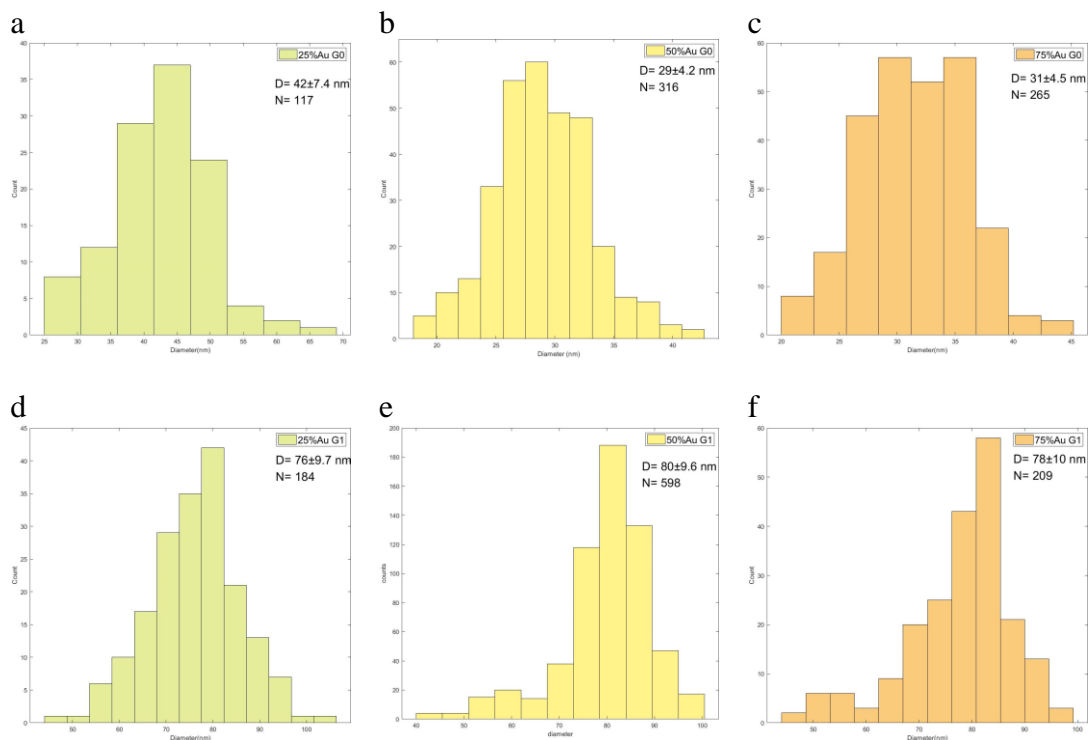


Figure 4. Nanoparticle size distribution of all samples by analysis of TEM images.

Numbers of analyzed nanoparticles are denoted as N. And the diameters of analyzed nanoparticles are denoted as D.

	mean diameters (nm)	max plasmonic peaks (nm)	Atomic% of Au*
25%Au G0	42±7.4	427	15.89
50%Au G0	29±4.2	458	45.51
75%Au G0	31±4.5	504	69.23
25%Au G1	76±9.7	464	12.83
50%Au G1	80±9.6	505	46.96
75%Au G1	78±10	533	69.40

* Atomic% of Au was estimated from EDAX spectra to track the trend of element content

change

Table 1. Average diameters and plasmonic peaks of Au-Ag alloy nanoparticles samples

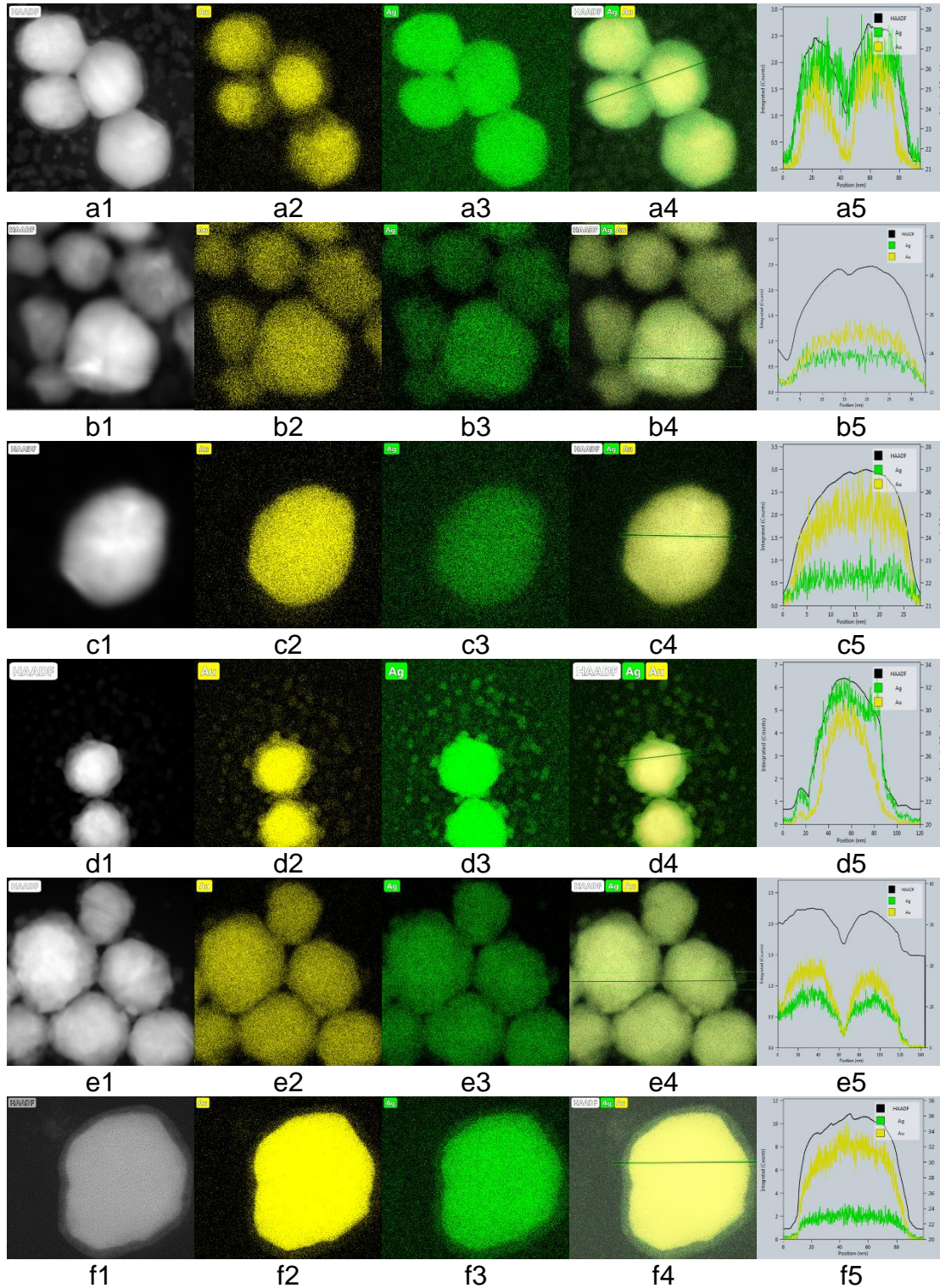


Figure 5. HAADF-STEM, EDAX-mapping and line-profiling of gold-silver alloy nanoparticles of representative 25%Au G0(a), 50%Au G0(b), 75%Au G0(c), 25%Au G1(d), 50%Au G1(e), 75%Au G1(f).

As mentioned previously, gold and silver have similar lattice constants and thus it is very difficult to distinguish between crystallites that consist of pure silver, pure gold or alloys within nanoparticles by electron diffraction¹⁹. To confirm the presence of gold-silver alloy nanoparticles, EDAX spectra were measured. Figure 5 shows HAADF-STEM images, EDAX's elemental mappings of gold, silver and both elements merged, as well as line profiling of the investigated nanoparticle. In all cases, the EDAX mapping shows a uniform distribution of gold and silver content within the cores of the investigated alloy nanoparticles, and the intensities for gold and silver correlates with HAADF's in EDAX line profiling spectra. However, when comparing the distribution of gold and silver with the line-profiling spectra from the EDAX mapping for 25% Au G0 and G1 nanoparticles (Figure 5a and 5d), there appears to be a fairly prominent silver-rich surface layer for these nanoparticles. This silver-rich surface shell is also visible in HAADF-STEM images due to silver's lower-contrast when compared to gold. Because silver is so strongly preferred at the surface, the EDAX intensity for silver in the core for these particles is smaller than expected for a particle that is only 25% gold in content.

A closer look also shows the presence of a silver-rich surface for 50% and 75% Au G0 and G1 nanoparticles, however this layer is much thinner and less prominent than for 25% Au nanoparticles. It is notable that the silver concentration is much higher within the surface region for all alloy nanoparticles (even for 75% Au G0 and G1 NPs), which was

revealed by line-profiling spectra of the different alloy nanoparticles in Figure 5. In bimetallic nanoparticles, the driving force for elemental segregation is the tendency to minimize the free energy of the nanoparticles. Viktoria et al reported the synthesis of 30-40 nm alloyed nanoparticle of gold-silver by coreduction⁴⁹, where HAADF-STEM images showed silver-rich patches within the investigated nanoparticle, indicating segregation between silver and gold within the synthesized nanoparticles. In contrast, here we observe that there is no clear separation between gold and silver in the cores of the nanoparticles. However, there is a clear preference for silver at the surface of the nanoparticles, which might be ascribed to differences in the surface energy⁶² or the reduction potential between silver and gold. The preferential presence of silver on the surface of gold-silver alloy nanoparticles was also reported by Guisbiers et al⁶². Although silver undergoes oxidation more easily than gold, the formation of silver oxide layers is unlikely in an aqueous environments⁶³.

2.4 Conclusion

In this work, we demonstrated a novel method for the synthesis of gold-silver alloy nanoparticles by the combination of seeded growth and citrate co-reduction of gold acetate and silver nitrate. The use of gold acetate as a precursor prevents the formation of insoluble AgCl during synthesis and allows for better control of the gold-silver ratio over a wider range of compositions. The prepared Au-Ag alloy seeds and large NPs are dispersed uniformly in size and shape and highly crystalline. Since the inexpensive and versatile citrate co-reduction method remains one of the best candidates for gold-silver alloy NPs preparation, the protocols described here would be very promising in future

industrial production as well as in potential biomedical and catalytic applications. For instance, El-Sayed and coworkers demonstrated the capability to directly image individual anti-EGFR-conjugated gold nanoparticles with dark field microscopy⁶⁴. With stronger scattering cross sections in theory¹³, our gold-silver alloy nanoparticles should be a better candidate for this type of biomedical application. Furthermore, the plasmonic resonance of these gold-silver alloy NPs can be tuned by controlling the size and composition of the alloy NPs. Alloy formation was confirmed by UV-Vis and EDAX spectra for all six samples. The uniform distributions of gold and silver content within the cores of the all Au-Ag alloy NPs are demonstrated by EDAX mapping and profiling. Notably, there appears to be a silver-rich surface for all synthesized alloy nanoparticles where this silver enriched surface layer is thicker and more prominent for 25% Au nanoparticles than for 50% and 75% Au nanoparticles. The clear preference for silver at the surface of Au-Ag alloy nanoparticles shown here needs more investigations and might be useful in the development of nanotechnologies where both silver surfaces and longer wavelength plasmon resonances are desired.

2.5 Reference

1. Bastús, N. G.; Comenge, J.; Puntès, V., Kinetically controlled seeded growth synthesis of citrate-stabilized gold nanoparticles of up to 200 nm: size focusing versus Ostwald ripening. *Langmuir* **2011**, *27* (17), 11098-11105.
2. Bastús, N. G.; Merkoçi, F.; Piella, J.; Puntès, V., Synthesis of highly monodisperse citrate-stabilized silver nanoparticles of up to 200 nm: kinetic control and catalytic properties. *Chemistry of Materials* **2014**, *26* (9), 2836-2846.
3. Ziegler, C.; Eychmüller, A., Seeded growth synthesis of uniform gold nanoparticles with diameters of 15– 300 nm. *The Journal of Physical Chemistry C* **2011**, *115* (11), 4502-4506.
4. Sarina, S.; Zhu, H.; Jaatinen, E.; Xiao, Q.; Liu, H.; Jia, J.; Chen, C.; Zhao, J., Enhancing catalytic performance of palladium in gold and palladium alloy nanoparticles for organic synthesis reactions through visible light irradiation at ambient temperatures. *Journal of the American Chemical Society* **2013**, *135* (15), 5793-5801.
5. Pan, Y.; Paschoalino, W. J.; Bayram, S. S.; Blum, A. S.; Mauzeroll, J., Biosynthesized silver nanorings as a highly efficient and selective electrocatalysts for CO₂ reduction. *Nanoscale* **2019**, *11* (40), 18595-18603.
6. Asapu, R.; Claes, N.; Bals, S.; Denys, S.; Detavernier, C.; Lenaerts, S.; Verbruggen, S. W., Silver-polymer core-shell nanoparticles for ultrastable plasmon-enhanced photocatalysis. *Applied Catalysis B: Environmental* **2017**, *200*, 31-38.
7. Smith, D. R.; Pendry, J. B.; Wiltshire, M. C., Metamaterials and negative refractive index. *Science* **2004**, *305* (5685), 788-792.
8. Zahr, O. K.; Blum, A. S., Solution phase gold nanorings on a viral protein template. *Nano letters* **2012**, *12* (2), 629-633.
9. Bayram, S. S.; Zahr, O. K.; Del Re, J.; Blum, A. S., Nanoring formation via in situ photoreduction of silver on a virus scaffold. *Nanotechnology* **2016**, *27* (48), 485603.
10. Petrescu, D. S.; Blum, A. S., Viral-based nanomaterials for plasmonic and photonic materials and devices. *Wiley Interdisciplinary Reviews: Nanomedicine and Nanobiotechnology* **2018**, *10* (4), e1508.
11. Cortie, M. B.; McDonagh, A. M., Synthesis and optical properties of hybrid and alloy plasmonic nanoparticles. *Chemical reviews* **2011**, *111* (6), 3713-35.
12. Barnes, W. L.; Dereux, A.; Ebbesen, T. W., Surface plasmon subwavelength optics. *Nature* **2003**, *424* (6950), 824-30.
13. Amendola, V.; Pilot, R.; Frascioni, M.; Maragò, O. M.; Iatì, M. A., Surface plasmon resonance in gold nanoparticles: a review. *Journal of Physics: Condensed Matter* **2017**, *29* (20), 203002.
14. Sotiriou, G. A.; Meyer, A.; Knijnenburg, J. T.; Panke, S.; Pratsinis, S. E., Quantifying the origin of released Ag⁺ ions from nanosilver. *Langmuir* **2012**, *28* (45), 15929-15936.
15. FDA, Over-the-counter drug products containing colloidal silver ingredients or silver salts. Department of Health and Human Services (HHS), Public Health Service (PHS), Food and Drug Administration (FDA). Final rule. *Fed Regist.* **1999**, *64*, 44653-44658.

16. Sotiriou, G. A.; Etterlin, G. D.; Spyrogianni, A.; Krumeich, F.; Leroux, J.-C.; Pratsinis, S. E., Plasmonic biocompatible silver–gold alloyed nanoparticles. *Chemical Communications* **2014**, *50* (88), 13559-13562.
17. Tiedemann, D.; Taylor, U.; Rehbock, C.; Jakobi, J.; Klein, S.; Kues, W. A.; Barcikowski, S.; Rath, D., Reprotoxicity of gold, silver, and gold–silver alloy nanoparticles on mammalian gametes. *Analyst* **2014**, *139* (5), 931-942.
18. Ristig, S.; Chernousova, S.; Meyer-Zaika, W.; Epple, M., Synthesis, characterization and in vitro effects of 7 nm alloyed silver–gold nanoparticles. *Beilstein journal of nanotechnology* **2015**, *6* (1), 1212-1220.
19. Mahl, D.; Diendorf, J.; Ristig, S.; Greulich, C.; Li, Z.-A.; Farle, M.; Köller, M.; Epple, M., Silver, gold, and alloyed silver–gold nanoparticles: characterization and comparative cell-biologic action. *Journal of Nanoparticle Research* **2012**, *14* (10), 1153.
20. Li, T.; Albee, B.; Alemayehu, M.; Diaz, R.; Ingham, L.; Kamal, S.; Rodriguez, M.; Bishnoi, S. W., Comparative toxicity study of Ag, Au, and Ag–Au bimetallic nanoparticles on *Daphnia magna*. *Analytical and bioanalytical chemistry* **2010**, *398* (2), 689-700.
21. Mallin, M. P.; Murphy, C. J., Solution-phase synthesis of sub-10 nm Au–Ag alloy nanoparticles. *Nano Letters* **2002**, *2* (11), 1235-1237.
22. Herbani, Y.; Nakamura, T.; Sato, S., Synthesis of near-monodispersed Au–Ag nanoalloys by high intensity laser irradiation of metal ions in hexane. *The Journal of Physical Chemistry C* **2011**, *115* (44), 21592-21598.
23. Shin, Y.; Dohnalkova, A.; Lin, Y., Preparation of homogeneous gold–silver alloy nanoparticles using the apoferritin cavity as a nanoreactor. *The Journal of Physical Chemistry C* **2010**, *114* (13), 5985-5989.
24. Hannemann, S.; Grunwaldt, J.-D.; Krumeich, F.; Kappen, P.; Baiker, A., Electron microscopy and EXAFS studies on oxide-supported gold–silver nanoparticles prepared by flame spray pyrolysis. *Applied surface science* **2006**, *252* (22), 7862-7873.
25. Gonzalez, C. M.; Liu, Y.; Scaiano, J., Photochemical strategies for the facile synthesis of gold–silver alloy and core–shell bimetallic nanoparticles. *The Journal of Physical Chemistry C* **2009**, *113* (27), 11861-11867.
26. Zhang, G.; Du, M.; Li, Q.; Li, X.; Huang, J.; Jiang, X.; Sun, D., Green synthesis of Au–Ag alloy nanoparticles using *Cacumen platycladi* extract. *RSC advances* **2013**, *3* (6), 1878-1884.
27. Ristig, S.; Prymak, O.; Loza, K.; Gocyla, M.; Meyer-Zaika, W.; Heggen, M.; Raabe, D.; Epple, M., Nanostructure of wet-chemically prepared, polymer-stabilized silver–gold nanoalloys (6 nm) over the entire composition range. *Journal of Materials Chemistry B* **2015**, *3* (23), 4654-4662.
28. Austin, L. A.; Kang, B.; El-Sayed, M. A., Probing molecular cell event dynamics at the single-cell level with targeted plasmonic gold nanoparticles: A review. *Nano Today* **2015**, *10* (5), 542-558.
29. Huang, X.; El-Sayed, I. H.; Qian, W.; El-Sayed, M. A., Cancer cell imaging and photothermal therapy in the near-infrared region by using gold nanorods. *Journal of the American Chemical Society* **2006**, *128* (6), 2115-2120.
30. Raschke, G.; Kowarik, S.; Franzl, T.; Sönnichsen, C.; Klar, T.; Feldmann, J.; Nichtl, A.; Kürzinger, K., Biomolecular recognition based on single gold nanoparticle light scattering. *Nano letters* **2003**, *3* (7), 935-938.

31. Sönnichsen, C.; Reinhard, B. M.; Liphardt, J.; Alivisatos, A. P., A molecular ruler based on plasmon coupling of single gold and silver nanoparticles. *Nature biotechnology* **2005**, *23* (6), 741-745.
32. Nan, X.; Sims, P. A.; Xie, X. S., Organelle tracking in a living cell with microsecond time resolution and nanometer spatial precision. *ChemPhysChem* **2008**, *9* (5), 707-712.
33. Kang, J. W.; So, P. T.; Dasari, R. R.; Lim, D.-K., High resolution live cell Raman imaging using subcellular organelle-targeting SERS-sensitive gold nanoparticles with highly narrow intranogap. *Nano letters* **2015**, *15* (3), 1766-1772.
34. Ando, J.; Fujita, K.; Smith, N. I.; Kawata, S., Dynamic SERS imaging of cellular transport pathways with endocytosed gold nanoparticles. *Nano letters* **2011**, *11* (12), 5344-5348.
35. Harmsen, S.; Huang, R.; Wall, M. A.; Karabeber, H.; Samii, J. M.; Spaliviero, M.; White, J. R.; Monette, S.; O'Connor, R.; Pitter, K. L., Surface-enhanced resonance Raman scattering nanostars for high-precision cancer imaging. *Science translational medicine* **2015**, *7* (271), 271ra7-271ra7.
36. Aslan, K.; Wu, M.; Lakowicz, J. R.; Geddes, C. D., Fluorescent core-shell Ag@ SiO₂ nanocomposites for metal-enhanced fluorescence and single nanoparticle sensing platforms. *Journal of the American Chemical Society* **2007**, *129* (6), 1524-1525.
37. Bharadwaj, P.; Novotny, L., Spectral dependence of single molecule fluorescence enhancement. *Optics Express* **2007**, *15* (21), 14266-14274.
38. Bharadwaj, P.; Novotny, L., Plasmon-enhanced photoemission from a single Y₃N@ C₈₀ fullerene. *The Journal of Physical Chemistry C* **2010**, *114* (16), 7444-7447.
39. Guerrero, A. R.; Zhang, Y.; Aroca, R. F., Experimental confirmation of local field enhancement determining far-field measurements with shell-isolated silver nanoparticles. *Small* **2012**, *8* (19), 2964-2967.
40. Asselin, J.; Legros, P.; Grégoire, A.; Boudreau, D., Correlating metal-enhanced fluorescence and structural properties in Ag@ SiO₂ core-shell nanoparticles. *Plasmonics* **2016**, *11* (5), 1369-1376.
41. Lehmuskero, A.; Johansson, P.; Rubinsztein-Dunlop, H.; Tong, L.; Kall, M., Laser trapping of colloidal metal nanoparticles. *ACS nano* **2015**, *9* (4), 3453-3469.
42. Hansen, P. M.; Bhatia, V. K.; Harrit, N.; Oddershede, L., Expanding the optical trapping range of gold nanoparticles. *Nano letters* **2005**, *5* (10), 1937-1942.
43. Ohlinger, A.; Nedev, S.; Lutich, A. A.; Feldmann, J., Optothermal escape of plasmonically coupled silver nanoparticles from a three-dimensional optical trap. *Nano letters* **2011**, *11* (4), 1770-1774.
44. Verbruggen, S. W.; Keulemans, M.; Martens, J. A.; Lenaerts, S., Predicting the surface plasmon resonance wavelength of gold-silver alloy nanoparticles. *The Journal of Physical Chemistry C* **2013**, *117* (37), 19142-19145.
45. LaMer, V. K.; Dinegar, R. H., Theory, production and mechanism of formation of monodispersed hydrosols. *Journal of the American Chemical Society* **1950**, *72* (11), 4847-4854.
46. LaMer, V. K., Nucleation in Phase Transitions. *Industrial & Engineering Chemistry* **1952**, *44* (6), 1270-1277.
47. Polte, J., Fundamental growth principles of colloidal metal nanoparticles—a new perspective. *CrytEngComm* **2015**, *17* (36), 6809-6830.

48. Link, S.; Wang, Z. L.; El-Sayed, M., Alloy formation of gold– silver nanoparticles and the dependence of the plasmon absorption on their composition. *The Journal of Physical Chemistry B* **1999**, *103* (18), 3529-3533.
49. Grasmik, V.; Rurainsky, C.; Loza, K.; Evers, M. V.; Prymak, O.; Heggen, M.; Tschulik, K.; Epple, M., Deciphering the surface composition and the internal structure of alloyed silver–gold nanoparticles. *Chemistry–A European Journal* **2018**, *24* (36), 9051-9060.
50. Blommaerts, N.; Vanrompay, H.; Nuti, S.; Lenaerts, S.; Bals, S.; Verbruggen, S. W., Unraveling structural information of Turkevich synthesized plasmonic gold–silver bimetallic nanoparticles. *Small* **2019**, *15* (42), 1902791.
51. Turkevich, J.; Stevenson, P. C.; Hillier, J., A study of the nucleation and growth processes in the synthesis of colloidal gold. *Discussions of the Faraday Society* **1951**, *11*, 55-75.
52. Rioux, D.; Meunier, M., Seeded Growth Synthesis of Composition and Size-Controlled Gold–Silver Alloy Nanoparticles. *The Journal of Physical Chemistry C* **2015**, *119* (23), 13160-13168.
53. Plowman, B. J.; Sidhureddy, B.; Sokolov, S. V.; Young, N. P.; Chen, A.; Compton, R. G., Electrochemical behavior of gold–silver alloy nanoparticles. *ChemElectroChem* **2016**, *3* (7), 1039-1043.
54. Navya, P.; Madhyastha, H.; Madhyastha, R.; Nakajima, Y.; Maruyama, M.; Srinivas, S.; Jain, D.; Amin, M. H.; Bhargava, S. K.; Daima, H. K., Single step formation of biocompatible bimetallic alloy nanoparticles of gold and silver using isonicotinylhydrazide. *Materials Science and Engineering: C* **2019**, *96*, 286-294.
55. Al-Zubeidi, A.; Stein, F.; Flatebo, C.; Rehbock, C.; Hosseini Jebeli, S. A.; Landes, C. F.; Barcikowski, S.; Link, S., Single-Particle Hyperspectral Imaging Reveals Kinetics of Silver Ion Leaching from Alloy Nanoparticles. *ACS nano* **2021**, *15* (5), 8363-8375.
56. Sakurai, H.; Koga, K.; Iizuka, Y.; Kiuchi, M., Colorless alkaline solution of chloride-free gold acetate for impregnation: An innovative method for preparing highly active Au nanoparticles catalyst. *Applied Catalysis A: General* **2013**, *462*, 236-246.
57. Hugon, A.; El Kolli, N.; Louis, C., Advances in the preparation of supported gold catalysts: Mechanism of deposition, simplification of the procedures and relevance of the elimination of chlorine. *Journal of Catalysis* **2010**, *274* (2), 239-250.
58. Ivanova, S.; Pitchon, V.; Zimmermann, Y.; Petit, C., Preparation of alumina supported gold catalysts: Influence of washing procedures, mechanism of particles size growth. *Applied Catalysis A: General* **2006**, *298*, 57-64.
59. Banerjee, M.; Sharma, S.; Chattopadhyay, A.; Ghosh, S. S., Enhanced antibacterial activity of bimetallic gold-silver core–shell nanoparticles at low silver concentration. *Nanoscale* **2011**, *3* (12), 5120-5125.
60. Lu, L.; Burkey, G.; Halaciuga, I.; Goia, D. V., Core–shell gold/silver nanoparticles: Synthesis and optical properties. *Journal of colloid and interface science* **2013**, *392*, 90-95.
61. Goudeli, E.; Pratsinis, S. E., Surface composition and crystallinity of coalescing silver–gold nanoparticles. *Acs Nano* **2017**, *11* (11), 11653-11660.
62. Guisbiers, G.; Mendoza-Cruz, R. n.; Bazán-Díaz, L.; Velázquez-Salazar, J. J. s.; Mendoza-Perez, R.; Robledo-Torres, J. A.; Rodriguez-Lopez, J.-L.; Montejano-Carrizales, J. M.; Whetten, R. L.; José-Yacamán, M. J. A. n., Electrum, the gold–silver alloy, from the bulk scale to the nanoscale: synthesis, properties, and segregation rules. *ACS nano* **2016**, *10* (1), 188-198.

63. Gallardo, O. A. D.; Moiraghi, R.; Macchione, M. A.; Godoy, J. A.; Pérez, M. A.; Coronado, E. A.; Macagno, V. A. J. R. a., Silver oxide particles/silver nanoparticles interconversion: susceptibility of forward/backward reactions to the chemical environment at room temperature. *RSC advances* **2012**, *2* (7), 2923-2929.
64. Yang, X.; Yang, M.; Pang, B.; Vara, M.; Xia, Y., Gold nanomaterials at work in biomedicine. *Chemical reviews* **2015**, *115* (19), 10410-10488.

Chapter 3. The dealloying of gold-silver alloy nanoparticles by BSPP towards porous nanostructures

3.1 Introduction

Porous nanostructures have become a popular domain for research by virtue of their desirable structures and properties that are different from their solid counterparts, making them popular in medical technology, chemistry, and materials science¹⁻⁴. The higher surface-to-volume ratio than similar solid structures makes porous nanomaterials versatile in drug delivery⁵, medical imaging⁶, and bio-sensors⁷. Furthermore, porous nanostructures that possess higher surface energy from more edges and corner sites have better performance in catalysis⁸. Plasmonic alloy nanoparticles are intermetallic compounds of metallic elements that have also generated enormous scientific interest because of their additional properties when compared to pure metals⁹. They have also been used to generate porous nanoparticles through selective removal of one component. For example, the porous plasmonic nanoparticles such as porous gold nanoparticles have been prepared from the dealloying of Au/Ag bi-layer films¹⁰, Ag₆₅Au₃₅ leaf¹¹ and Au-Ag alloy ingots¹². Although gold is usually viewed as an inert metal, porous Au nanoparticles are catalytically active for several heterogeneous oxidation reactions¹³. However, Au is the only transition metal with an endothermic chemisorption energy for oxygen, which indicates that it does not readily bind oxygen molecules¹³. Investigation of the intrinsic catalysis mechanism of gold nanoparticles thus requires the preparation of non-supported porous gold nanoparticles to avoid the influence of oxygen binding to the support.

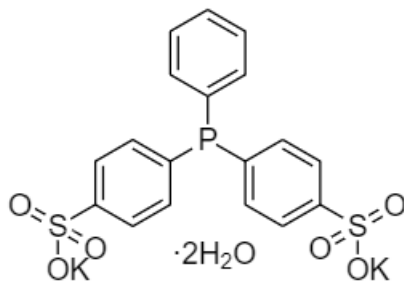


Figure 1. Chemical structure of Bis(p-sulfonatophenyl)phenylphosphine dihydrate dipotassium dehydrate salt.

Bis(p-sulfonatophenyl)phenylphosphine (BSPP) is a water-soluble derivative of triphenylphosphine that has been commonly used in the synthesis of gold nanoparticles¹⁴. BSPP coordinates with Ag^+ to form a stable complex¹⁵. Since silver nanoparticles release Ag^+ ions upon contact with water¹⁶⁻¹⁸, it is anticipated that the release of Ag^+ ions from silver nanoparticles will be facilitated with the help of BSPP in the solution through Ag^+ -BSPP complex formation. Meanwhile, BSPP is an excellent stabilizer for gold nanoparticles¹⁹⁻²¹. Therefore, we aim at dealloying gold-silver alloy nanoparticles with selective silver etching to form a porous gold nanostructure, which requires the dissolution of silver and the complexation of silver ions by BSPP as well as the stabilization of gold by BSPP.

In this chapter, we demonstrate the preparation of unsupported porous alloy nanostructures in the presence of excess BSPP. While silver does not appear to be selectively removed from alloy nanoparticles, TEM shows the presence of small

nanoparticles forming on the surface of the larger alloy nanoparticles. Energy-dispersive X-ray spectroscopy (EDX) indicates that these small outer nanoparticles are mainly comprised of silver, resulting in large central alloy core particles surrounded by smaller silver satellite nanoparticles with high surface area. The formation of these core-satellite particles is monitored by UV-Vis spectroscopy and transmission electron microscopy (TEM).

3.2 Experimental

3.21 Materials

All chemicals were used without further purification. BSPP (Sigma-Aldrich), Gold (III) acetate (99.9%, Alfa Aesar), silver nitrate (>99%, Sigma-Aldrich), and sodium citrate (Sigma-Aldrich). Deionized (DI) water (>18 M Ω *cm) was used and obtained using Barnstead Diamond TII (Thermo Fisher) purification system. Centrifugations were performed with a SORVALL RC 6 PLUS centrifuge (Thermo Fisher Scientific, Waltham, MA) using a SH-3000 swinging rotor.

3.22 Synthesis of gold-silver alloy nanoparticles

The synthesis protocol of gold-silver alloy nanoparticles was described in the experimental section of Chapter 2.

3.23 Dealloying process

The alloy nanoparticles solution was centrifuged for 45 minutes and redispersed in an equal volume of deionized water before the dealloying reaction. The molar ratio between

BSPP and metal (Au+Ag) was set as $X = 2$. Briefly, BSPP was added into 1 mL of alloy nanoparticle solution in a 1.5 mL microcentrifuge tube. Next, the microcentrifuge tube was vortexed for about 1 minutes and wrapped by aluminum foil to protect it from light excitation, waiting for further characterization such as UV-Vis and TEM measurements.

3.24 Instrumentation

UV-visible spectra in the 350-700 nm region were collected using a Cary 100 Bio instrument. The size, morphology and size distribution were characterized by TEM (Philips CM200 TEM). EDX-mapping was conducted on FEI Tecnai G2 F20 STEM. All of the UV-Vis data were processed by MATLAB. Measurements in TEM images were conducted with ImageJ Software. The structure of BSPP is drawn in ChemDraw.

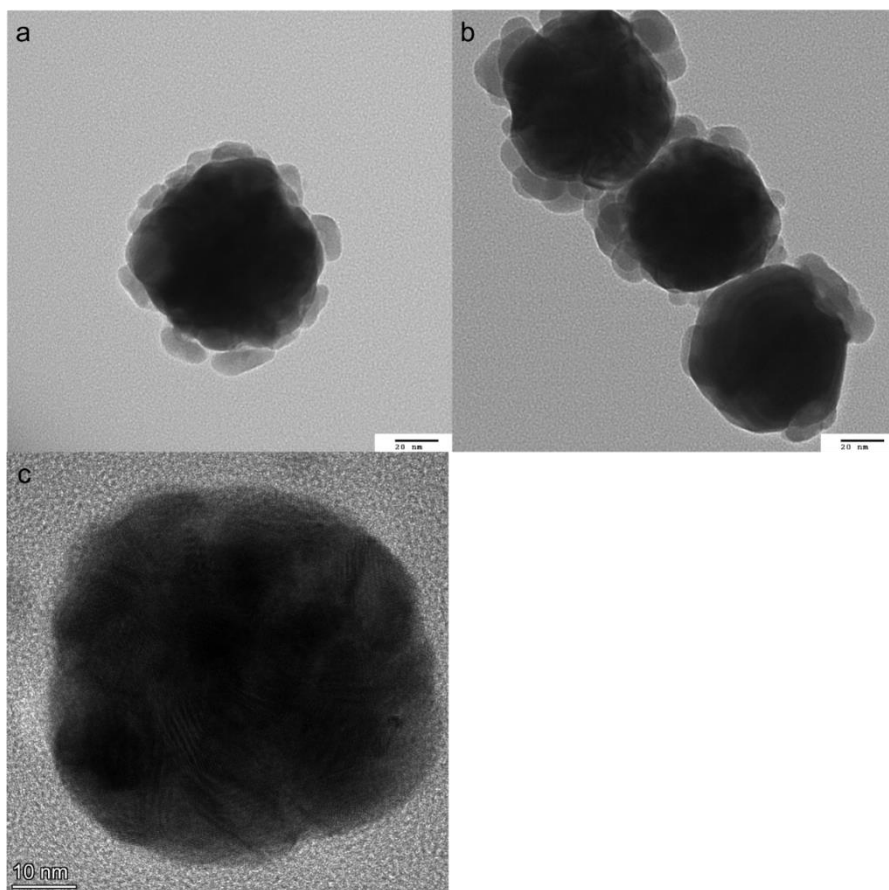


Figure 2. TEM images of 50%Au G1 nanoparticles (a) after 26 hours treatment with BSPP (X=2) and (b) after 56 hours treatment of BSPP (X=2) and (c) before BSPP treatment.

3.3 Results and Discussion

The TEM images of 50%Au G1 alloy nanoparticles treated with BSPP (X=2) after 26 hours and 56 hours are presented on Figure 2. The diameters of these (center) nanoparticles are 80.10 ± 8.12 nm (26 hours treatment) and 74.79 ± 5.80 nm (56 hours treatment). Since the diameter of 50%Au G1 alloy nanoparticles (before BSPP treatment) is 80 ± 9.6 nm, it is possible that there is no size shrinkage of nanoparticles after BSPP treatment and the center nanoparticles are porous. The central core nanoparticles are surrounded by much smaller nanoparticles, with much lower TEM contrast (intensity) than the core nanoparticles. After 56 hours of BSPP treatment, the outer nanoparticles are larger in size than those 26 hours of BSPP treatment, which may imply that dealloying continues over time. Since the contrast of particles imaged in TEM increases roughly with higher atomic number squared²² (Z^2), silver nanoparticles have lower TEM contrast than gold nanoparticles. The large difference in contrast between the smaller satellite particles and the larger core particle suggests that there is much more silver in the satellite particles.

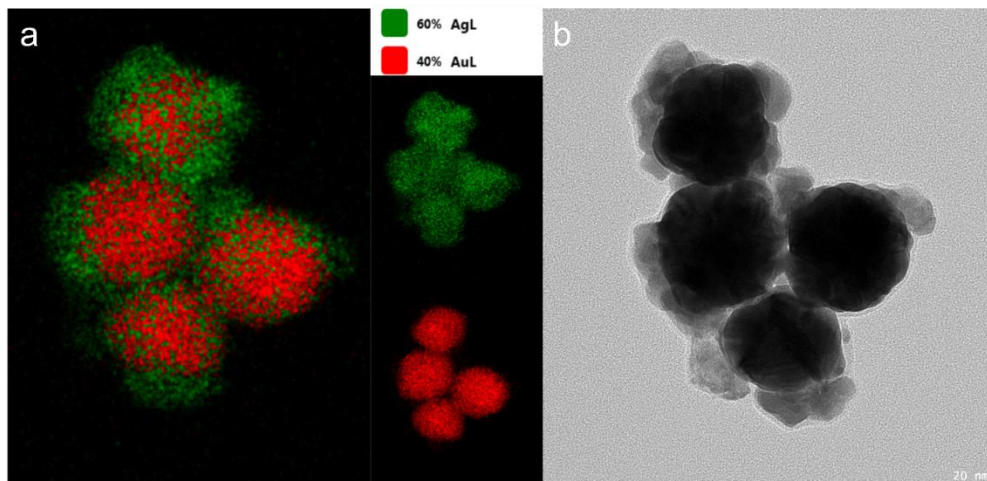


Figure 3. (a) EDX-mapping spectra (acquired on STEM mode) of 50%Au G1 nanoparticles with the addition of BSPP after 56 hours. Red pixels represent gold and green pixels represent silver. (b) TEM images of the corresponding 50%Au G1 nanoparticles measured by EDX-mapping. Please note that due to instrument limitations, there are positional deviations between the images acquired on STEM and TEM modes.

Figure 3 shows 50%Au G1 alloy nanoparticles after 56 hours BSPP treatment imaged and analyzed by EDX and TEM. Given that BSPP stabilizes gold nanoparticles and forms coordination complexes with Ag^+ , and that the large contrast difference suggests that the satellite particles are mostly comprised of silver, we used EDX-mapping to look at the spatial distribution of gold and silver in the core-satellite structures. EDX confirms that the outer nanoparticles are mainly composed of silver rather than gold. Both silver and gold are present in the larger core nanoparticle, although the intensity for gold is much higher. The overall EDX intensity reflects a 60:40 Ag:Au ratio that is consistent with the synthesis composition of 50 Au G1 nanoparticles, implying that the silver of the satellite particles originates from the starting alloy nanoparticles.

Inspired by a mechanistic study of silver nanoprism growth¹⁵, a proposed reaction mechanism of silver deposition on the center nanoparticle is shown in Figure 4. First, the release of silver ions is facilitated by BSPP. Since citrate anions bind to both gold and silver nanoparticles²³, it is expected that the alloy nanoparticles (the yellow sphere on Figure 4) are surrounded with citrate anions after synthesis, and the alloy nanoparticles could be partially negative charged as a result. The negatively charged particles could donate an electron to a silver cation that is complexed by BSPP. As more Ag^+ are reduced back to Ag^0 , more silver atoms aggregate on the surface of alloy nanoparticles resulting in silver satellite particles while the citrate anions are oxidated into acetoacetate and carbon dioxide.

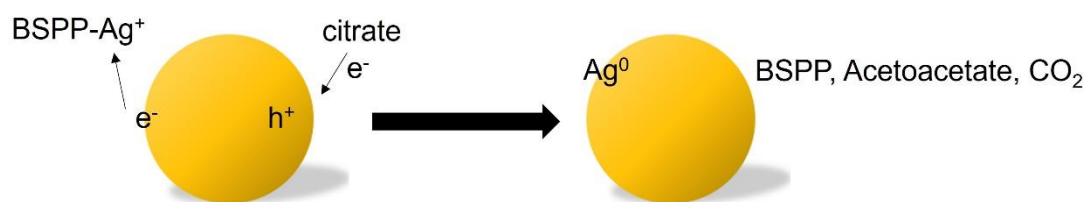


Figure 4. Scheme of the proposed reaction mechanism of silver deposition on the center nanoparticle. The yellow sphere stands for the alloy nanoparticle.

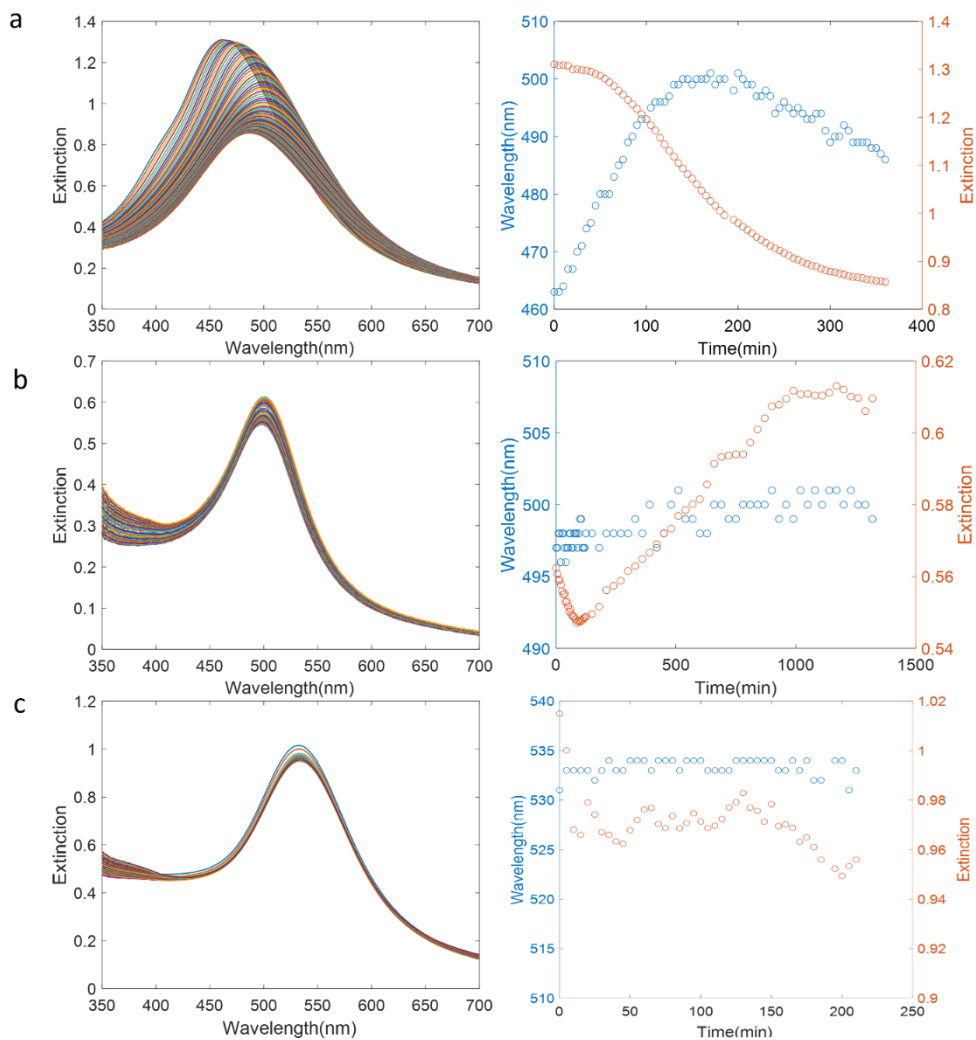


Figure 5. The extinction spectra of gold-silver alloy nanoparticles in the presence of excessive BSPP ($X=2$) over time (left images) and the corresponding changes (right images) of maximum extinction intensity (orange plots and axis) and maximum plasmonic peaks wavelength (blue plots and axis) over time. (a) 25%Au G1 nanoparticles scanned per 5 minutes for 360 minutes. (b) 50%Au G1 nanoparticles scanned per 5 minutes for 0-125 minutes and per 30 minutes for 150-1320 minutes. (c) 75%Au G1 nanoparticles scanned per 5 minutes for 210 minutes.

To investigate the effect of alloy composition on the dealloying process, a kinetic study with G1 alloy nanoparticles from 25%Au to 75%Au is conducted by UV-Vis spectroscopy. Since the maximum extinction intensity and its corresponding maximum plasmonic peak wavelength are related to the plasmonic nanoparticle's structure, composition, size and local environment, the following discussion will be focused on these two parameters from the UV-Vis spectra. In Figure 5a, the maximum peak wavelength for 25%Au G1 starts at 463 nm at time 0, reaches a plateau at 500 nm from 140 to 230 minutes, and then shifts to 486 nm at 360 minutes. It is noticeable that the peak maxima first undergo a red-shift and then a blue-shift. The red-shift could be attributed to an increase in the fraction of gold in the alloy nanoparticle (Figure 4), in the alloy nanoparticle (Figure 5), given that the plasmonic peak for 80 nm gold nanoparticles is 546.5 nm²⁴, while that for silver is 460 nm²⁵. As shown in chapter 2, as the fraction of gold in an alloy nanoparticle increases, the plasmon resonance position red shifts. The blue-shift could result from the formation of the satellite nanoparticles that contain mainly silver. Meanwhile, the maximum extinction intensity decreases from 1.31 to 0.86, which may be due to the incomplete reduction of silver ions complexed by BSPP. And the maximum extinction intensity may reach a plateau with extended time. Throughout the whole time period of the study, there is a single plasmon resonance, implying that the satellite nanoparticles do not behave like a complete shell on the core alloy particle. For a complete shell, we would expect to see a secondary plasmonic resonance^{26, 27}.

In Figure 5b, the maximum peak wavelengths for 50%Au G1 fluctuate within the range of 496 nm to 501 nm. It is possible that the core composition does not change much over the time of the experiment, with most of the removed silver coming from the outer

areas of the nanoparticle. This seems likely, given the results from chapter 2, which show that our alloy particles are enriched in silver at the surface for all alloy compositions. The changes in the maximum extinction intensity over time follow a “V” shape trend with an initial decrease to a turning point is at (85, 0.55), followed by an increase to a plateau at 990 minutes with the intensity around 0.61. This could reflect initial depletion of silver from the alloy nanoparticle followed by deposition of silver as satellite nanoparticles. Since silver nanoparticles have higher surface plasmonic resonance intensity than gold²⁸, as silver is removed, gold has a stronger influence on the maximum extinction intensity of 50%Au G1 nanoparticles, which leads to a decrease of the maximum extinction intensity. Once enough silver redeposits on the core, silver’s influence increases again and generates an increase in the maximum extinction intensity. In Figure 5c, both the maximum peak wavelengths and the maximum extinction intensity of 75%Au G1 nanoparticles are nearly unchanged, which demonstrates that the 75%Au G1 nanoparticles are not very active for dealloying. In light of the magnitude of changes in maximum peak wavelengths and maximum extinction intensities within the same time scale (Table 1), 25%Au G1 will readily undergo dealloying, while 75%Au G1 will barely change in the same time, with 50%Au G1 in between. Additional follow up is required to confirm these results, including TEM at more time points. Dark field scattering spectroscopy may be helpful to further characterize these materials.

	Δ Peak Max (nm)	Δ Extinction
25%Au G1	38	0.339
50%Au G1	1	0.06
75%Au G1	2	0.006

Table 1. The difference between the maximum peak wavelengths and maximum extinction intensity at 0 minute and 210 minutes.

3.4 Preliminary Conclusion and Future Work

Citrate capped 50%Au G1 alloy nanoparticles undergo dealloying in the presence of BSPP, yielding a novel nanostructure where the central core alloy nanoparticles are surrounded with small satellite nanoparticles. EDX-mapping results demonstrates that the satellite nanoparticles are mainly composed of silver and the central core nanoparticles contain more gold than silver. Guided by the TEM and EDX results, we present a proposed dealloying mechanism. In addition, the dealloying of 25%Au G1, 50%Au G1 and 75%Au G1 nanoparticles with BSPP is monitored by UV-Vis spectroscopy over time. 25%Au G1 is the most active for dealloying while 75%Au G1 is the least active, which may be due to differences in the amount of silver ions formed at the nanoparticle surface.

Further evidence provided by TEM, EDX-mapping and UV-Vis as well as control experiments are required to demonstrate the mechanism, optimal reaction conditions, and applications of the reported dealloying reaction. It is expected that the outer nanoparticles could be removed by nitric acid which dissolves silver but is passive to gold. Although the TEM data suggests that there is not a significant loss in size upon etching with BSPP, and thus the particles are porous, this needs additional confirmation. The porosity of the center nanoparticles could be measured by BET surface area analysis. Preliminary results suggest that we have a versatile method for the preparation of stable porous alloy nanoparticles, and that the degree of etching (and thus porosity) can be

controlled by the gold-silver ratio in the alloy particles. Particles with higher silver content are more readily etched by BSPP, as expected. Further work is required to build on these encouraging results.

3.5 Reference

1. Gao, Y.; Zhao, Y.; Liu, H.; Shao, M.; Chen, Z.; Ma, T.; Wu, Z.; Wang, L., N, P-doped carbon supported ruthenium doped Rhenium phosphide with porous nanostructure for hydrogen evolution reaction using sustainable energies. *Journal of Colloid and Interface Science* **2022**, *606*, 1874-1881.
2. Wang, X.; Chen, F.; Yang, M.; Guo, L.; Xie, N.; Kou, X.; Song, Y.; Wang, Q.; Sun, Y.; Lu, G., Dispersed WO₃ nanoparticles with porous nanostructure for ultrafast toluene sensing. *Sensors and Actuators B: Chemical* **2019**, *289*, 195-206.
3. Liu, Y.; Yan, X.; Xu, B.; Lan, J.; Yu, Y.; Yang, X.; Lin, Y.; Nan, C., Self-reconstructed formation of a one-dimensional hierarchical porous nanostructure assembled by ultrathin TiO₂ nanobelts for fast and stable lithium storage. *ACS applied materials & interfaces* **2018**, *10* (22), 19047-19058.
4. Zeng, H.; Cai, W.; Liu, P.; Xu, X.; Zhou, H.; Klingshirn, C.; Kalt, H., ZnO-based hollow nanoparticles by selective etching: elimination and reconstruction of metal– semiconductor interface, improvement of blue emission and photocatalysis. *ACS nano* **2008**, *2* (8), 1661-1670.
5. Li, J.; Wu, S.; Wu, C.; Qiu, L.; Zhu, G.; Cui, C.; Liu, Y.; Hou, W.; Wang, Y.; Zhang, L., Versatile surface engineering of porous nanomaterials with bioinspired polyphenol coatings for targeted and controlled drug delivery. *Nanoscale* **2016**, *8* (16), 8600-8606.
6. Luo, M.; Xu, L.; Xia, J.; Zhao, H.; Du, Y.; Lei, B., Synthesis of porous gadolinium oxide nanosheets for cancer therapy and magnetic resonance imaging. *Materials Letters* **2020**, *265*, 127375.
7. Han, T.; Cao, Y.; Chen, H.-Y.; Zhu, J.-J., Versatile porous nanomaterials for electrochemiluminescence biosensing: Recent advances and future perspective. *Journal of Electroanalytical Chemistry* **2021**, *902*, 115821.
8. Bhanja, P.; Modak, A.; Bhaumik, A., Supported porous nanomaterials as efficient heterogeneous catalysts for CO₂ fixation reactions. *Chemistry–A European Journal* **2018**, *24* (29), 7278-7297.
9. Cortie, M. B.; McDonagh, A. M., Synthesis and optical properties of hybrid and alloy plasmonic nanoparticles. *Chemical reviews* **2011**, *111* (6), 3713-3735.
10. Wang, D.; Schaaf, P., Nanoporous gold nanoparticles. *Journal of Materials Chemistry* **2012**, *22* (12), 5344-5348.
11. Fujita, T.; Guan, P.; McKenna, K.; Lang, X.; Hirata, A.; Zhang, L.; Tokunaga, T.; Arai, S.; Yamamoto, Y.; Tanaka, N., Atomic origins of the high catalytic activity of nanoporous gold. *Nature materials* **2012**, *11* (9), 775-780.
12. Wittstock, A.; Zielasek, V.; Biener, J.; Friend, C.; Bäumer, M., Nanoporous gold catalysts for selective gas-phase oxidative coupling of methanol at low temperature. *Science* **2010**, *327* (5963), 319-322.
13. Hvolbæk, B.; Janssens, T. V.; Clausen, B. S.; Falsig, H.; Christensen, C. H.; Nørskov, J. K., Catalytic activity of Au nanoparticles. *Nano today* **2007**, *2* (4), 14-18.
14. Weare, W. W.; Reed, S. M.; Warner, M. G.; Hutchison, J. E., Improved synthesis of small (d core \approx 1.5 nm) phosphine-stabilized gold nanoparticles. *Journal of the American Chemical Society* **2000**, *122* (51), 12890-12891.

15. Xue, C.; Métraux, G. S.; Millstone, J. E.; Mirkin, C. A., Mechanistic study of photomediated triangular silver nanoprism growth. *Journal of the American Chemical Society* **2008**, *130* (26), 8337-8344.
16. Sotiriou, G. A.; Meyer, A.; Knijnenburg, J. T.; Panke, S.; Pratsinis, S. E., Quantifying the origin of released Ag⁺ ions from nanosilver. *Langmuir* **2012**, *28* (45), 15929-15936.
17. Navarro, E.; Piccapietra, F.; Wagner, B.; Marconi, F.; Kaegi, R.; Odzak, N.; Sigg, L.; Behra, R., Toxicity of silver nanoparticles to *Chlamydomonas reinhardtii*. *Environmental science & technology* **2008**, *42* (23), 8959-8964.
18. Kittler, S.; Greulich, C.; Diendorf, J.; Koller, M.; Epple, M., Toxicity of silver nanoparticles increases during storage because of slow dissolution under release of silver ions. *Chemistry of materials* **2010**, *22* (16), 4548-4554.
19. Li, Z.; Cheng, E.; Huang, W.; Zhang, T.; Yang, Z.; Liu, D.; Tang, Z., Improving the yield of mono-DNA-functionalized gold nanoparticles through dual steric hindrance. *Journal of the American Chemical Society* **2011**, *133* (39), 15284-15287.
20. Wu, R.; Jiang, L.-P.; Zhu, J.-J.; Liu, J., Effects of small molecules on DNA adsorption by gold nanoparticles and a case study of tris (2-carboxyethyl) phosphine (TCEP). *Langmuir* **2019**, *35* (41), 13461-13468.
21. Fernandes, R.; Smyth, N. R.; Muskens, O. L.; Nitti, S.; Heuer-Jungemann, A.; Arden-Jones, M. R.; Kanaras, A. G., Interactions of skin with gold nanoparticles of different surface charge, shape, and functionality. *Small* **2015**, *11* (6), 713-721.
22. Fultz, B.; Howe, J. M., *Transmission electron microscopy and diffractometry of materials*. Springer Science & Business Media: 2012.
23. Park, J.-W.; Shumaker-Parry, J. S., Structural study of citrate layers on gold nanoparticles: role of intermolecular interactions in stabilizing nanoparticles. *Journal of the American Chemical Society* **2014**, *136* (5), 1907-1921.
24. Bastús, N. G.; Comenge, J.; Puentes, V., Kinetically controlled seeded growth synthesis of citrate-stabilized gold nanoparticles of up to 200 nm: size focusing versus Ostwald ripening. *Langmuir* **2011**, *27* (17), 11098-11105.
25. Bastús, N. G.; Merkoçi, F.; Piella, J.; Puentes, V., Synthesis of highly monodisperse citrate-stabilized silver nanoparticles of up to 200 nm: kinetic control and catalytic properties. *Chemistry of Materials* **2014**, *26* (9), 2836-2846.
26. Gonzalez, C. M.; Liu, Y.; Scaiano, J., Photochemical strategies for the facile synthesis of gold–silver alloy and core–shell bimetallic nanoparticles. *The Journal of Physical Chemistry C* **2009**, *113* (27), 11861-11867.
27. Banerjee, M.; Sharma, S.; Chattopadhyay, A.; Ghosh, S. S., Enhanced antibacterial activity of bimetallic gold-silver core–shell nanoparticles at low silver concentration. *Nanoscale* **2011**, *3* (12), 5120-5125.
28. Amendola, V.; Pilot, R.; Frasconi, M.; Maragò, O. M.; Iatì, M. A., Surface plasmon resonance in gold nanoparticles: a review. *Journal of Physics: Condensed Matter* **2017**, *29* (20), 203002.

Chapter 4. Investigation of the optical properties of gold-silver alloy nanoparticles with dark-field hyperspectral microscopy

4.1 Introduction

Dark-field microscopy has been used in recent years for monitoring chemical reactions¹⁻³, biosensing⁴⁻⁷, and molecule detection⁸. Dark-field microscopy is based on indirect sample illumination where only scattered light from the sample is captured⁹. The primary advantage of this technique is that it provides high contrast images and makes it possible to collect the scattering light of plasmonic nanoparticles at the single-particle level¹⁰. Unlike in bright-field illumination, where the specimen is illuminated by a directly-focused light to produce dark images on a white background, in dark-field microscopy only peripheral light illuminates the specimen while the direct light is cut off by the light stop, resulting in bright images on a black (dark) background¹¹. Due to the Tyndall effect, where light is scattered by particles roughly between 40 and 900 nm in a colloid, nanoparticles that are much smaller than the typical optical microscope resolution limit (0.6 μm – 0.2 μm) can be visualized using dark-field microscopy. Hyperspectral imaging (HSI) is a technique allowing for the acquisition of two-dimensional images across a range of the electromagnetic spectrum¹². This technique is based on images produced while collecting the whole spectrum per image pixel, instead of taking a photograph where each pixel is dominated by a single wavelength (as happens in normal microphotography)¹³. HSI used along with dark-field microscopy could offer significant advantages for rapid label-free spatially-resolved detection and characterization of nanoparticles¹⁴. Figure 1 provides a generalized scheme of the system and the data acquisition device¹⁵.

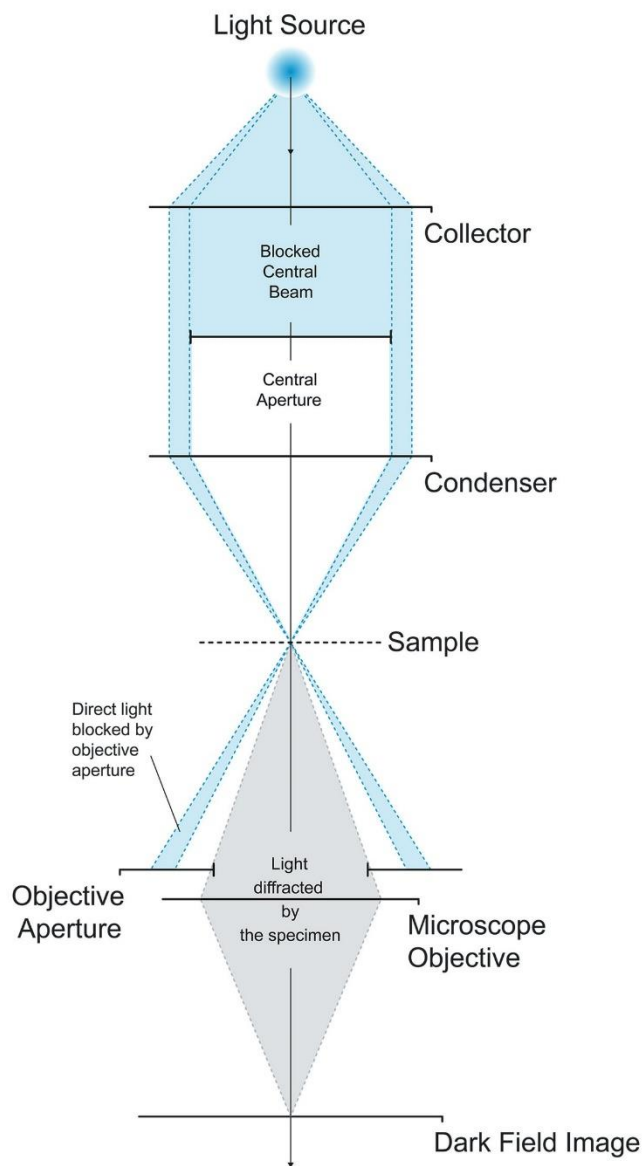


Figure 1. Generalized scheme of darkfield microscopy. This diagram is acquired from Photon etc¹⁶. (Montreal, Quebec, Canada) and a copyrighted work of Photon etc.

Owing to the characteristic localized surface plasmon resonance, plasmonic nanoparticles scatter light very strongly: scattering light from single silver or gold NPs larger than 20 nm diameter can be easily seen under a microscope¹⁷. As a characteristic

optical spectroscopy technique, dark-field microscopy coupled with a spectrometer has been developed for the observation and measurement of the UV-Vis-NIR spectrum of plasmonic nanoparticles at the single particle level. Plasmonic nanoparticles yield strong light scattering in dark-field microscopy imaging because of enhanced light absorption and scattering by surface plasmons¹⁸ and thus can be visualized as bright spots with the characteristic plasmonic color on a dark background¹⁹. The wavelength of the scattered light is directly related to the surface plasmons of the nanoparticle and its size, shape, material, and local environment. The detection of silver nanoparticles with diameters exceeding 5 nm has been reported using dark-field hyperspectral microscopy²⁰. With the employment of dark-field hyperspectral microscopy, it is possible to investigate the scattered light of individual gold-silver alloy nanoparticles with different ratios of gold to silver.

A theory describing scattering and absorption of light by spherical nanoparticles was proposed by Mie, also known as Mie scattering²¹. Assuming that small spherical nanoparticles interact with a plane wave incident, the extinction and the total scattering cross sections can be expressed as²¹:

$$\sigma_{\text{ext}} = \frac{18\pi\epsilon_m^{3/2} V}{\lambda} \frac{\epsilon_2(\lambda)}{[\epsilon_1(\lambda) + 2\epsilon_m]^2 + \epsilon_2(\lambda)^2}$$

$$\sigma_{\text{sca}} = \frac{32\pi^4 \epsilon_m^2 V^2}{\lambda^4} \frac{(\epsilon_1 - \epsilon_m)^2 + (\epsilon_2)^2}{[\epsilon_1 + 2\epsilon_m]^2 + (\epsilon_2)^2}$$

Where V is the particle volume, and $\epsilon_m = n_m^2$ is the medium's dielectric function, and ϵ_1 and ϵ_2 are the real and imaginary parts of the metal dielectric index respectively. λ is the wavelength of the incident light. For noble metal nanoparticles (Au, Ag and Cu), with a negative real and small positive imaginary dielectric constant over a range of wavelengths, the surface plasmon resonance frequency occurs in the visible to near-infrared region²².

In this chapter, we report light scattering measurements of our synthesized gold-silver alloy nanoparticles at the single nanoparticle level by our dark-field hyperspectral microscope. This study is at a very early stage and aims at investigating how uniform our alloy nanoparticles are with respect to element distributions and compositions. It is expected that the results from this study will be complementary to the UV-Visible extinction spectra and TEM results discussed in Chapter 2. Though the results of this study are preliminary, we demonstrate that dark field scattering measurements on gold-silver alloy particles will be useful in determining the optical characteristics of individual nanoparticles, which can then be compared to our previous ensemble measurements.

4.2 Experimental

4.21 Materials

All chemicals were used without further purification. Hydrogen Peroxide (30%, Thermo Fisher), Sulfuric Acid (95-98%, Thermo Fisher), Acetone (HPLC grade, Thermo Fisher), Gold (III) acetate (99.9%, Alfa Aesar), silver nitrate (>99%, Sigma-Aldrich), and sodium citrate (Sigma-Aldrich). Deionized (DI) water (>18 M Ω *cm) was used and obtained using Barnstead Diamond TII (Thermo Fisher) purification system. Centrifugations were

performed with a SORVALL RC 6 PLUS centrifuge (Thermo Fisher Scientific, Waltham, MA) using a SH-3000 swinging rotor.

4.22 Synthesis of gold-silver alloy nanoparticles

The synthesis protocol of gold-silver alloy nanoparticles was described in the experiment section of Chapter 2.

4.23 Instrumentation

Dark-field hyperspectral microscopy characterization: The dark-field image and light scattering spectra were measured on a hyperspectral dark-field microscope (IMA, Photon etc., Canada). This microscope was equipped with a Nikon ECLIPSE Ti2-U Inverted Microscope, Hamamatsu ORCA-Flash4.0 V3 sCMOS Camera, and NKT Photonics SuperK FIANIUM FIU-15 Supercontinuum Laser (tunable on the range of 400-1000 nm with a spectral resolution of about 2 nm). Each light scattering spectra was acquired on 9 pixel and the image time on laser was 0.2 second under a 20x objective. The scattering spectra were recorded per 10 nm of laser per pixel and the samples were surrounded with air at room temperature after pure nitrogen drying. The spectra were processed by MATLAB software.

4.24 Glass slide pretreatment and sample preparation

The procedure for glass slide cleaning was developed by my lab mate, Alexander Al-Feghali. Briefly, piranha solution was prepared in a beaker with extreme caution. The as-prepared piranha solution was added into a Coplin jar with glass slides. And the jar was sonicated for 90 minutes. The piranha solution was removed into a beaker and neutralized by sodium bicarbonate. Next, the glass slides in the jar were rinsed with deionized water and HPLC grade acetone. The Coplin jar was filled with HPLC grade acetone and sonicated for 10 minutes. Then the Coplin jar was refilled with another batch of HPLC grade acetone and the glass slides waited for further use. And the imaging nanoparticles were immobilized on glass slides by drop-casting. The excessive solution was removed by nitrogen drying.

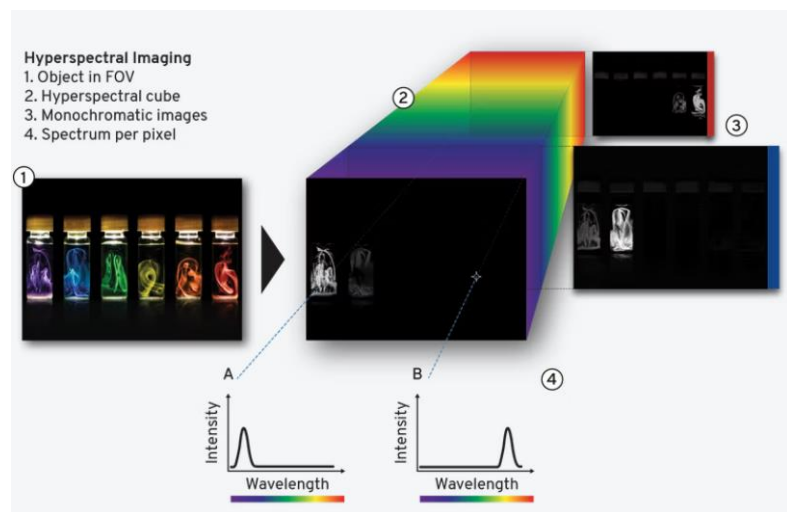


Figure 2. Schematic of a hyperspectral data cube. This scheme is acquired from Photon etc²³. (Montreal, Quebec, Canada) and a copyrighted work of Photon etc.

4.3 Results and Discussion

In our dark-field microscope, each hyperspectral measurement will generate a hyperspectral data cube, which consists of a subset of its spatial and spectral information per pixel²³ (Figure 2). Figure 3 shows typical dark-field images of our synthesized gold-silver alloy nanoparticles from 25%Au G0 to 75%Au G1 in white light mode. The alloy nanoparticles with different gold-silver ratios are well dispersed as small diffraction limited “bright white spots” in the field of view. Figure 4 shows dark-field hyperspectral images acquired at 600 nm of laser light, which has much lower signal to noise, as shown by the brighter background. The hyperspectral images are shown in greyscale and relative to the current image intensity at different wavelength of laser light, where the “bright spots” denotes gold-silver alloy nanoparticles. The formation of some larger bright spots on the images could be attributed to nanoparticle aggregations or coherent artifacts²⁴.

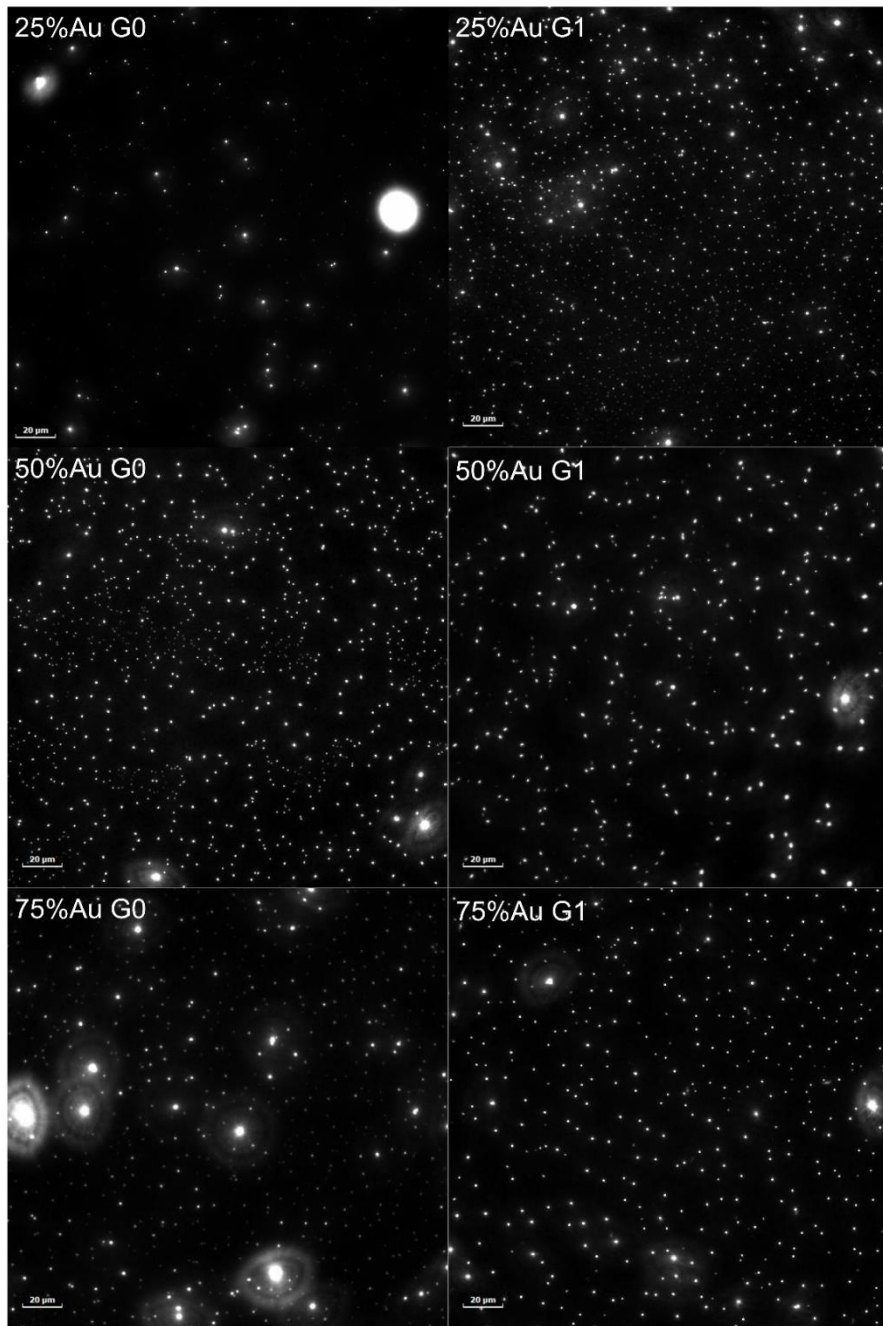


Figure 3. Dark-field images of gold-silver alloy nanoparticles from 25% Au G0 to 75% Au G1.

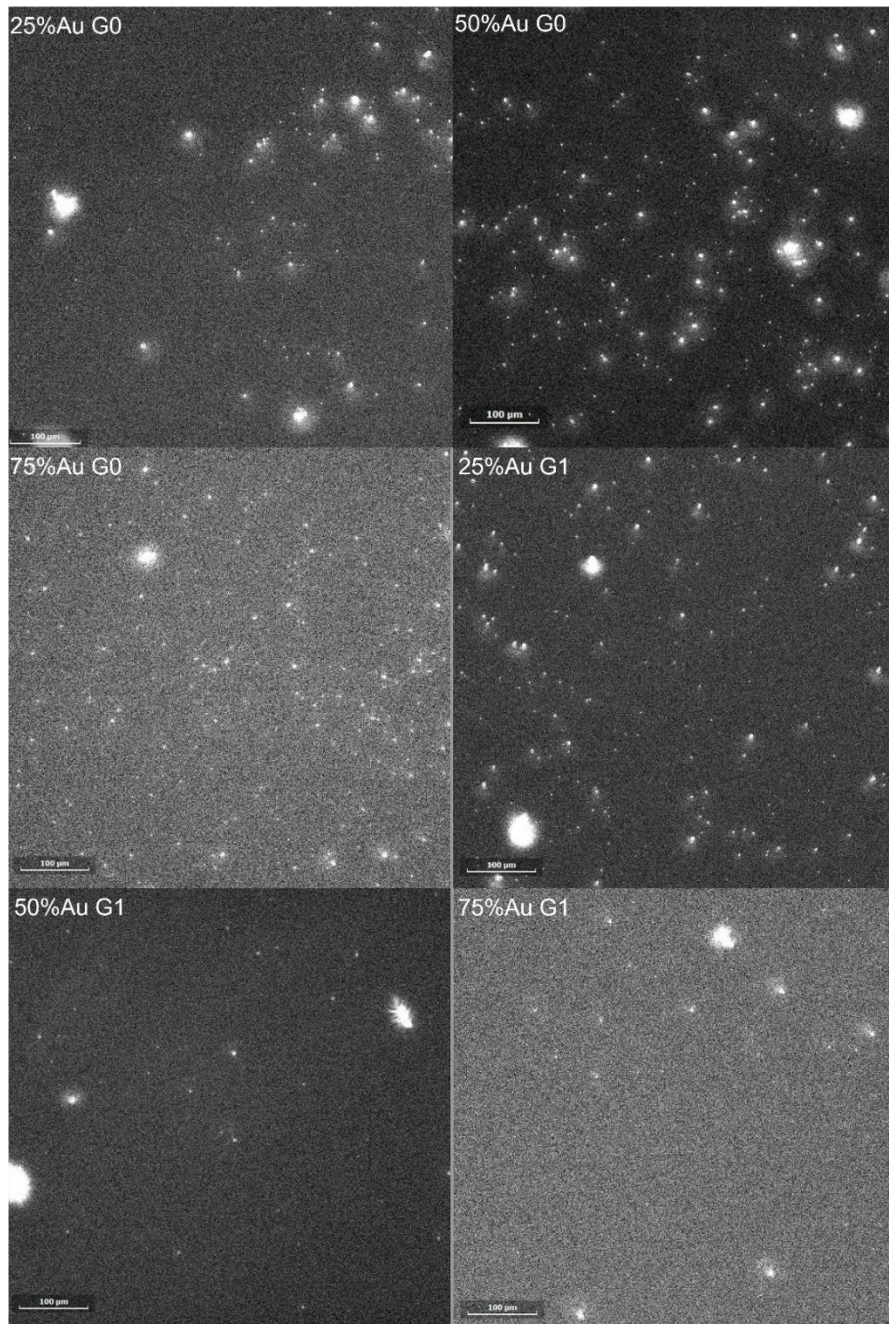


Figure 4. Dark-field hyperspectral image of gold-silver alloy nanoparticles from 25% Au G0 to 75% Au G1 at 600 nm of laser.

Typical scattering spectra scanned from 400 nm to 1000 nm for gold-silver alloy nanoparticles of G0 and G1 with different gold-silver ratios are shown in Figure 5 as well as summarized in Table 1. Scattered light from gold-silver alloy nanoparticles provides information about the nanoparticles' composition, size and local environment. Due to the instrumental and operational limitations, the scattering signals of individual nanoparticles are recorded per 10 nm of laser wavelength and the scattering signals are not stable due to a poor signal to noise ratio, which is shown by the different background whiteness in Figure 4 and the relatively large standard deviations of the scattering intensity as shown in Table 1.

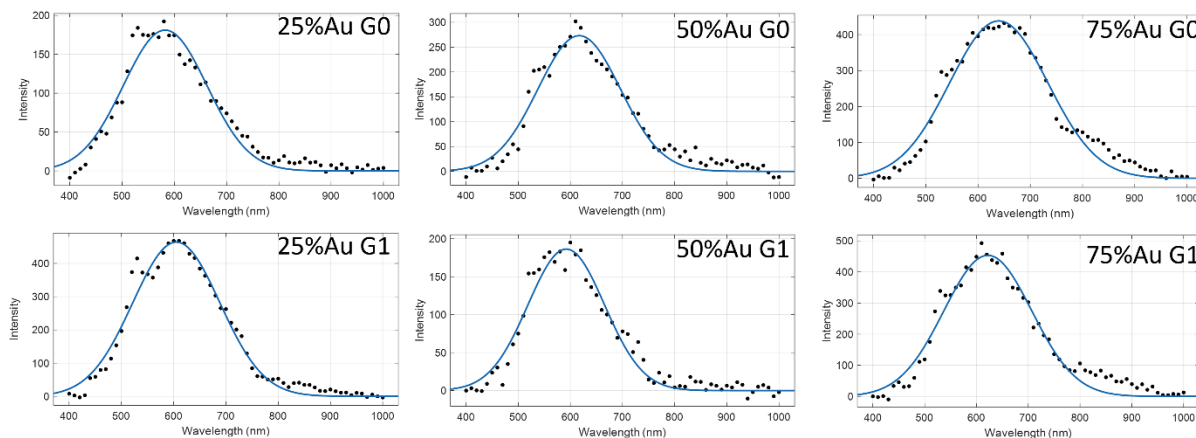


Figure 5. Typical scattering spectra of gold-silver alloy nanoparticles (G0 and G1) with different ratio of gold to silver. The blue lines are the Gaussian fittings of the spectra.

It is anticipated that there will be peaks in the scattering spectra that are similar to the peaks in their corresponding extinction spectra measured by UV-Visible spectroscopy. The FWHM (full width half-maximum) value is an estimate of the sharpness of the

scattering spectra. Our FWHM results suggest that the G1 alloy nanoparticles are more uniform than the G0 alloy nanoparticles, which is also revealed by the smaller standard deviations of the G1 alloy nanoparticles' maximum scattering intensity. 25 Au G0 is the least uniform alloy sample. The peaks of maximum scattering intensity are red-shifted around 100 nm compared to their counterparts in extinction spectra, which is due to different local dielectric environment or nanoparticles aggregations, as the aggregations of silver nanoparticles could lead to a large spectral red-shift (102 nm)²⁵. As expected, the plasmon resonance redshifts with an increase in the ratio of gold in the alloy nanoparticles, with the exception of 50 Au G1 nanoparticles. This is similar to the trend observed for the peaks in their corresponding extinction spectra in solution as described in Chapter 2. Previous theoretical scattering spectra demonstrate that larger nanoparticles have higher scattering efficiency and longer wavelengths of maximum scattering intensity²⁶. Overall, as the diameters of alloy nanoparticles increase (from G0 to G1), the scattering intensity of nanoparticles with the same gold-silver ratio increases and the peaks red-shift. Meanwhile, it is noticeable that there are shoulder peaks appearing at 800 – 1000 nm, most apparently for the 75 Au G0 and 75 Au G1 alloy nanoparticles, which requires further investigation.

It is expected that the scattering spectra of plasmonic nanoparticles at the individual particle level are not completely uniform, with the different composition and size of each nanoparticle affecting the observed plasmon resonance. Jing et al.²⁷ report that maximum in scattering for three gold nanoparticles from the same dark-field image are 540 nm, 580 nm and 620 nm. Therefore, we will need to acquire more scattering spectra from hundreds of alloy nanoparticles to conduct statistics analysis in order to reveal how

uniform our alloy nanoparticles are with respect to composition and element distribution in individual nanoparticles.

	Peak Max (nm)	Intensity	Number of Spectra	Full Width at Half Maximum
25%Au G0	562 ± 35	157 ± 161	17	111 ± 74
50%Au G0	587 ± 13	361 ± 254	15	179 ± 9
75%Au G0	608 ± 23	270 ± 201	17	193 ± 26
25%Au G1	605 ± 15	473 ± 261	15	184 ± 11
50%Au G1	592 ± 18	224 ± 116	14	183 ± 11
75%Au G1	627 ± 13	322 ± 150	13	181 ± 11

Table 1. Summary of scattering spectra of gold-silver alloy nanoparticles.

4.4 Preliminary Conclusion and Future Work

In this chapter, we present the images of our synthesized gold-silver alloy nanoparticles with different gold-silver ratio by dark-field hyperspectral microscopy both in white light and laser mode. In addition, the light scattering spectra of alloy nanoparticles are shown and the trends of them are mostly aligned with the ones of our UV-Visible extinction spectra described in Chapter 2. The peaks redshifts with an increase in gold content, with the exception of 50 Au G1 nanoparticles. The G1 alloy nanoparticles have longer peak wavelengths than the corresponding G0 alloy nanoparticles because of their larger diameters. Although the sample preparation needs to be better optimized and the issue with the laser power in our dark-field microscope needs to be resolved, our preliminary data suggests that darkfield scattering will be useful to answer the question of how uniform our synthesized gold-silver alloy nanoparticles really are. With more

measurement and analysis, it is anticipated that the conclusions drawn from our scattering spectra of alloy nanoparticles and this characterization method based on dark-field microscopy developed from our research group will be beneficial for the development of alloy nanomaterial science.

4.5 References

1. Novo, C.; Funston, A. M.; Mulvaney, P., Direct observation of chemical reactions on single gold nanocrystals using surface plasmon spectroscopy. *Nature Nanotechnology* **2008**, *3* (10), 598-602.
2. Novo, C.; Funston, A. M.; Gooding, A. K.; Mulvaney, P., Electrochemical Charging of Single Gold Nanorods. *Journal of the American Chemical Society* **2009**, *131* (41), 14664-14666.
3. Jing, C.; Gu, Z.; Xie, T.; Long, Y.-T., Color-coded imaging of electrochromic process at single nanoparticle level. *Chemical Science* **2016**, *7* (8), 5347-5351.
4. Lee, K.; Cui, Y.; Lee, L. P.; Irudayaraj, J., Quantitative imaging of single mRNA splice variants in living cells. *Nature Nanotechnology* **2014**, *9* (6), 474-480.
5. Xu, X.; Li, T.; Xu, Z.; Wei, H.; Lin, R.; Xia, B.; Liu, F.; Li, N., Automatic Enumeration of Gold Nanomaterials at the Single-Particle Level. *Analytical Chemistry* **2015**, *87* (5), 2576-2581.
6. Xu, X.; Chen, Y.; Wei, H.; Xia, B.; Liu, F.; Li, N., Counting Bacteria Using Functionalized Gold Nanoparticles as the Light-Scattering Reporter. *Analytical Chemistry* **2012**, *84* (22), 9721-9728.
7. Liu, Y.; Huang, C. Z., Real-Time Dark-Field Scattering Microscopic Monitoring of the in Situ Growth of Single Ag@Hg Nanoalloys. *ACS Nano* **2013**, *7* (12), 11026-11034.
8. Shi, L.; Jing, C.; Ma, W.; Li, D. W.; Halls, J. E.; Marken, F.; Long, Y. T., Plasmon resonance scattering spectroscopy at the single-nanoparticle level: real-time monitoring of a click reaction. *Angewandte Chemie International Edition* **2013**, *52* (23), 6011-6014.
9. Xiao, L.; Yeung, E. S., Optical Imaging of Individual Plasmonic Nanoparticles in Biological Samples. *Annual Review of Analytical Chemistry* **2014**, *7* (1), 89-111.
10. Liu, M.; Chao, J.; Deng, S.; Wang, K.; Li, K.; Fan, C., Dark-field microscopy in imaging of plasmon resonant nanoparticles. *Colloids and Surfaces B: Biointerfaces* **2014**, *124*, 111-117.
11. Davidson, M. W.; Abramowitz, M., Optical microscopy. *Encyclopedia of imaging science and technology* **2002**, *2* (1106-1141), 120.
12. Giannoni, L.; Lange, F.; Tachtsidis, I., Hyperspectral imaging solutions for brain tissue metabolic and hemodynamic monitoring: past, current and future developments. *Journal of Optics* **2018**, *20* (4), 044009.
13. Roth, G. A.; Tahiliani, S.; Neu-Baker, N. M.; Brenner, S. A., Hyperspectral microscopy as an analytical tool for nanomaterials. *Wiley Interdisciplinary Reviews: Nanomedicine and Nanobiotechnology* **2015**, *7* (4), 565-579.
14. Fakhrullin, R.; Nigmatzyanova, L.; Fakhrullina, G., Dark-field/hyperspectral microscopy for detecting nanoscale particles in environmental nanotoxicology research. *Science of The Total Environment* **2021**, *772*, 145478.
15. Zamora-Perez, P.; Pelaz, B.; Tsoutsis, D.; Soliman, M. G.; Parak, W. J.; Rivera-Gil, P., Hyperspectral-enhanced dark field analysis of individual and collective photo-responsive gold-copper sulfide nanoparticles. *Nanoscale* **2021**, *13* (31), 13256-13272.
16. Glossary in Optics & Photonics. <https://www.photonetc.com/glossary-in-optics-and-photonics>.

17. Wang, X.; Zhang, Z.; Hartland, G. V., Electronic Dephasing in Bimetallic Gold–Silver Nanoparticles Examined by Single Particle Spectroscopy. *The Journal of Physical Chemistry B* **2005**, *109* (43), 20324-20330.
18. Sriram, M.; Markhali, B. P.; Nicovich, P. R.; Bennett, D. T.; Reece, P. J.; Hibbert, D. B.; Tilley, R. D.; Gaus, K.; Vivekchand, S.; Gooding, J. J., A rapid readout for many single plasmonic nanoparticles using dark-field microscopy and digital color analysis. *Biosensors and Bioelectronics* **2018**, *117*, 530-536.
19. Jain, P. K.; Huang, X.; El-Sayed, I. H.; El-Sayed, M. A., Noble Metals on the Nanoscale: Optical and Photothermal Properties and Some Applications in Imaging, Sensing, Biology, and Medicine. *Accounts of Chemical Research* **2008**, *41* (12), 1578-1586.
20. Théoret, T.; Wilkinson, K. J., Evaluation of enhanced darkfield microscopy and hyperspectral analysis to analyse the fate of silver nanoparticles in wastewaters. *Analytical Methods* **2017**, *9* (26), 3920-3928.
21. Mayer, K. M.; Hafner, J. H., Localized surface plasmon resonance sensors. *Chemical reviews* **2011**, *111* (6), 3828-3857.
22. Li, T.; Wu, X.; Liu, F.; Li, N., Analytical methods based on the light-scattering of plasmonic nanoparticles at the single particle level with dark-field microscopy imaging. *Analyst* **2017**, *142* (2), 248-256.
23. Hyperspectral Imaging. <https://www.photonetc.com/hyperspectral-imaging>.
24. Patskovsky, S.; Bergeron, E.; Meunier, M., Hyperspectral darkfield microscopy of PEGylated gold nanoparticles targeting CD44-expressing cancer cells. *Journal of biophotonics* **2015**, *8* (1-2), 162-167.
25. Sönnichsen, C.; Reinhard, B. M.; Liphardt, J.; Alivisatos, A. P., A molecular ruler based on plasmon coupling of single gold and silver nanoparticles. *Nature biotechnology* **2005**, *23* (6), 741-745.
26. Patskovsky, S.; Bergeron, E.; Rioux, D.; Simard, M.; Meunier, M., Hyperspectral reflected light microscopy of plasmonic Au/Ag alloy nanoparticles incubated as multiplex chromatic biomarkers with cancer cells. *Analyst* **2014**, *139* (20), 5247-5253.
27. Jing, C.; Gu, Z.; Ying, Y.-L.; Li, D.-W.; Zhang, L.; Long, Y.-T., Chrominance to dimension: a real-time method for measuring the size of single gold nanoparticles. *Analytical chemistry* **2012**, *84* (10), 4284-4291.

Chapter 5. Concluding Remarks and Future Directions

This thesis concerns the synthesis, silver etching, and characterization by dark-field microscope of gold-silver alloy nanoparticles. In the first research project (Chapter Two), we report a novel two-step method for the synthesis of uniform quasi-spherical and monodisperse gold-silver alloy nanoparticles with diameters around 80 nm. In step one, gold-silver alloy seeds (G0) with diameters around 30 nm are synthesized by citrate co-reduction of gold acetate and silver nitrate. In step two, the seeds grow into large alloy nanoparticles with diameters around 80 nm by the combination of seeded growth and citrate co-reduction of gold and silver precursors. Our method makes use of gold acetate (rather than chloroauric acid) as a gold precursor to avoid the formation of silver chloride precipitates during synthesis. To our knowledge, we are the first to prepare gold-silver alloy nanoparticles with diameters above 70 nm using gold acetate as a gold precursor. The alloy seeds and seed grown nanoparticles show good control of size and composition, which enables tuning of the plasmonic band of these gold-silver alloy nanoparticles. Gold and silver are distributed uniformly within the cores of all Au-Ag alloy nanoparticles, while the surface is enriched in silver. This silver enriched surface layer is thicker and more prominent for 25% Au alloy nanoparticles than for 50% and 75% Au alloy nanoparticles.

The second research project (Chapter Three) investigates the etching of our synthesized gold-silver alloy nanoparticles by BSPP. This project was inspired by the mechanistic study¹ of photo-mediated triangular silver nanoprism growth. TEM and EDX measurements show that a novel nanostructure is formed after etching, where smaller silver nanoparticles were deposited on the surface of gold-silver alloy nanoparticles. The

proposed reaction mechanism consists of two steps: First, silver dissolution is facilitated by BSPP and a BSPP-Ag⁺ complex is formed; Second, the gold-silver alloy nanoparticle surface acts as a catalyst to facilitate the reduction of silver cations by nearby citrate ions. EDX-mapping results on 50% Au G1 nanoparticles demonstrate that the satellite nanoparticles are mainly composed of silver while the central core nanoparticles contain more gold than silver. In addition, the dealloying of 25%Au G1, 50%Au G1 and 75%Au G1 nanoparticles with BSPP is monitored by UV-Vis spectroscopy over time. 25%Au G1 is the most active for dealloying while 75%Au G1 is the least active, which may be due to differences in the amount of silver ions formed at the nanoparticle surface. Although TEM data suggests that there is not a significant loss in size upon etching with BSPP, and thus the particles are porous, this needs additional confirmation.

In the third research project (Chapter Four), we present our preliminary results of light scattering measurements of our synthesized gold-silver alloy nanoparticles with dark-field hyperspectral microscopy at the individual nanoparticle level. This study is at a very early stage and aims at investigating how uniform our alloy nanoparticles really are with respect to element distributions. Through the preliminary results of this study, light scattering spectra of alloy nanoparticles are shown and their trends are mostly aligned with the ones of our UV-Visible extinction spectra described in Chapter 2. The peaks redshift with an increase in gold content, with the exception of 50 Au G1 nanoparticles. The G1 alloy nanoparticles have longer peak wavelengths than the corresponding G0 alloy nanoparticles because of their larger diameters.

The future work on our gold-silver alloy nanoparticles includes the broader application of our synthesis method, such as attempting to synthesize alloy nanoparticles

with lower silver or gold content than reported in Chapter 2. The biocompatibility of our alloy nanoparticles should be examined by cell viability experiments. For the etching of alloy nanoparticles by BSPP, further evidence provided by TEM, EDX-mapping and UV-Vis as well as control experiments are required to demonstrate the mechanism, optimal reaction conditions, and applications of the reported dealloying reaction. In addition, BET measurements are required to measure the surface area of the novel core-satellite nanostructures to demonstrate their porosity. For the light scattering study of alloy nanoparticles by dark-field microscopy, sample preparation needs to be better optimized and the issue with the laser power in our dark-field microscope needs to be resolved. More scattering spectra from hundreds of alloy nanoparticles are essential to conduct statistical analysis to reveal the compositional uniformity of our alloy nanoparticles. Overall, it is anticipated that our reported synthesis method of gold-silver alloy nanoparticles, the preparation of core-satellite nanostructures by BSPP etching and the light scattering study by dark-field microscope are beneficial for the advancement of alloy nanomaterial science.

Reference

1. Xue, C.; Métraux, G. S.; Millstone, J. E.; Mirkin, C. A., Mechanistic study of photomediated triangular silver nanoprism growth. *Journal of the American Chemical Society* **2008**, *130* (26), 8337-8344.